Lego Chemistry: The Synthesis Of Microporous Materials

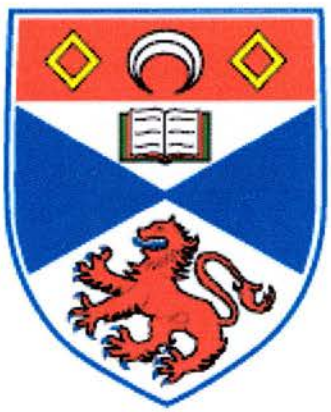

Lynsey Victoria Parke B.Sc.

University of St.Andrews

August 2003

Declarations

I, Lynsey Victoria Parke, hereby certify that this thesis, which is approximately 16000 words in length, has been written by me, that it is the record of work carried out by me and that it has not been submitted in any previous application for a higher degree.

Date 26/08/2003 signature of candidate

I was admitted as a research student in September, 2002 and as a candidate for the degree of M.Phil in September 2002; the higher study for which this is a record was carried out in the University of St Andrews between 2002 and 2003.

Date 26/08/2003 signature of candidate

I hereby certify that the candidate has fulfilled the conditions of the Resolution and Regulations appropriate for the degree of M.Phil in the University of St Andrews and that the candidate is qualified to submit this thesis in application for that degree.

Date 21/11/03 signature of supervisor

In submitting this thesis to the University of St Andrews I understand that I am giving permission for it to be made available for use in accordance with the regulations of the University Library for the time being in force, subject to any copyright vested in the work not being affected thereby. I also understand that the title and abstract will be published, and that a copy of the work may be made and supplied to any bona fide library or research worker.

Date 26/08/2003 signature of candidate

Courses Attended

The School of Chemistry at St.Andrews requires that a postgraduate attend a number of taught courses. The courses attended were:

- Crystallography Dr. P. Lightfoot
- Electrochemistry Dr. J. A. Crayston

Acknowledgements

I would like to thank Prof. Russell Morris for his supervision during this project. I would also like to thank Dr. Paul Wheatley for all his time and help and Dr. Simon Teat for his technical help while at the SRS in Daresbury. Thanks also to the Morris lab group; especially Dr. Chris Andrews, Dr. Meredith Hearshaw and Ewan Drylie for making the year enjoyable.

Thanks also to my parents, my brother Jeffers and sister Mels for all their help and support. Thanks to my friends throughout the year, especially everyone who was with me in St.Andrews who helped make it a fantastic one: Cyn, Ali, Liam and Beth.

Finally I would like to thank the School of Chemistry for the funding of this M.Phil project.

Abstract

The aim of this research project was to utilise the double-four rings, D4Rs, in the synthesis of crystalline microporous materials. These D4Rs are examples of pre-nucleation building units and have been investigated by Férey *et al.* The concept for this type of research involves using double-four rings as the starting material, which will bond together to form extended architectures that incorporate part of or wholly consist of the original unit. The products recovered were characterised by single-crystal and powder X-ray diffraction.

Several methods were investigated to produce microporous solids using these D4Rs, with structure-directing agents and organic/inorganic linkers to try and yield positive results. Solids incorporating the starting ingredients for the gallium cube; gallium phosphate, pyridine, phosphoric acid and H_2O, produced needle and rhomboidal prism crystals. After analysis at the synchrotron radiation source at Daresbury, they were shown to have pyridine located within the pores of the crystal. The needle crystals produced a large unit cell, a=8.905(2) Å, b=17.9133(4) Å and c=9.092(2) Å, compared to the rhomboidal prism crystals. However, no complete D4R units were contained within these structures.

Divalent metal ion compounds including barium, copper, calcium, and zinc were used next as linkers between the cubes. However, despite running experiments at room temperature and at 150 ^{0}C, no crystalline materials were produced, only gel-like solids. Mercury incorporated crystals, produced from mercury chloride added to the silica based cube dissolved in methanol, gave two crystal structures. Similar to the first reaction, needle-like and platelet crystals were produced, with unit cell volumes of

1047.46(79) $Å^3$ and 218.87(23) $Å^3$ respectively. Samples were also produced from organic linkers such as dipyridine dihydrochloride and imidazole hydrochloride with the $GaPO_4$ D4R unit. Cyclam, 1,4,8,11-tetraazacyclotetradecane, was also used as a metal-organic linker. Crystals incorporating these materials have not yet undergone X-ray diffraction analysis.

Table of Contents

1.0	INTRODUCTION	1
1.1	Microporous materials	1
1.1.1	Zeolite	2
1.1.2	Molecular sieve	3
1.2	Zeolite Structures	5
1.3	The Phosphates	8
1.3.1	Aluminophosphates	8
1.3.2	Gallophosphates	10
1.4	Uses of zeolites	11
1.4.1	Catalysis	12
1.4.2	Gas Separation	14
1.4.3	Ion Exchange	15
1.5	The Building Blocks	15
1.6	The Double Four Rings: D4Rs	18
1.7	Synthesis	22
1.8	References	24
2.0	AIMS	27
2.1	Synthesis of Microporous Materials using D4Rs	27
2.2	Linking the D4Rs	27
2.3	Using other 2+ ions	30

2.4 Cyclam: 1,4,8-Tetraazacyclotetradecane 30

2.5 References 33

3.0 EXPERIMENTAL TECHNIQUES 34

3.1 Hydrothermal Synthesis 34

3.2 X-ray Diffraction 34

3.2.1 Single crystal X-Ray Diffraction 38

3.2.2 Powder X-ray Diffraction 39

3.3 Synchrotron Radiation 40

3.4 References 43

4.0 EXPERIMENTAL 44

4.1 Preparation of the cubes 44

4.1.1 Tetramethylammonium Silica cube 45

4.1.2 Gallium Phosphate cube 45

4.1.3 Germanate cube 46

4.2 Variations on the Synthesis 47

4.3 TMA Silica based cube experiments 47

4.4 Incorporating $HgCl_2$ – Mercuric Chloride 48

4.5 Experimenting with other Mercury Compounds 49

4.6 Experiments involving Group II ions 50

4.7 Reactions at higher temperatures 54

4.8 The Gallium Phosphate cubes 55

4.9 The Introduction of Cyclam 56

4.9.1 References 59

5.0 RESULTS AND CONCLUSIONS 60

5.1 Introduction: Synthesising the starting materials 60

5.2 $GaPO_4$ cube under hydrothermal synthesis at high T 62

5.2.1 Powder X-ray Diffraction 62

5.2.2 Synchrotron radiation 63

5.2.3 Monoclinic Crystal 64

5.2.4 Conclusion 70

5.2.5 Rhomboidal Prism Crystal 70

5.2.6 Analysis of the crystal 71

5.2.7 Conclusion 75

5.3 A new approach to linking – Metal Ions 76

5.4 Mercury incorporated crystals 78

5.4.1 Needle Crystal 79

5.4.2 Conclusion 83

5.4.3 Platelet crystal 83

5.4.4 Conclusion 86

5.5 Organic Groups: Dipy and Imidazole Hydrochloride crystals 86

5.5.1 Single crystal X-ray diffraction 87

5.5.2 Dipyridine dihydrochloride crystal in CH_3OH 88

5.5.3 Conclusion 89

5.6 Gallium Phosphate crystals 89

5.6.1 Single crystal X-ray diffraction 89

5.6.2 $GaPO_4$ cube data 90

5.6.3 Conclusion 91

5.7 $GaPO_4$ incorporating cyclam and Imidazole Hydrochloride 92

5.8 The Germanate Cube 92

5.9 References 93

6.0 FURTHER WORK 94

7.0 APPENDIX 97

7.1 Crystal Data: Stan 194/lvp3n 98

7.2 Crystal Data: Stan 198/lvp3p 101

7.3 Crystal Data: lprm3n 103

7.4 Crystal Data: lprm3p 106

7.5 Crystal Data: lprm4 106

7.6 Crystal Data: lprm6 108

7.7 Figure 50 – lvp3 110

7.8 Figure 51 – lvp16on 111

7.9 Figure 52 – $HgCl_2$ 111

7.10 Figure 53 – lvp51 112

1.0 Introduction

1.1 Microporous Materials

It was in 1756 that the Swedish mineralogist Axel Frederick Cronstedt, discovered a natural mineral which visibly lost water when heated. He named the class of materials as zeolites, from the classical Greek words meaning 'boiling stones'.[1]

However it was in 1932 that the term 'molecular sieve' was proposed by McBain[2] to describe a class of materials that exhibited interesting properties such as selective adsorption. It was proposed that for a material to be termed a molecular sieve, 'it must separate components of a mixture on the basis of molecular size and shape differences'.

At this stage two classes of molecular sieve were known: the zeolites and certain microporous charcoals. Now we know other names that can be added to the list. The silicates, metallosilicates, metalloaluminates, the $AlPO_4$'s and silica- and metalloaluminophosphates are widely recognised materials. Their regular nanoporous framework structure will separate and discriminate components of a mixture on the basis of size and shape. The difference between a molecular sieve and zeolite lies not within the structure itself, but within their elemental composition. Therefore, all are molecular sieves though none but the aluminosilicates should carry the classical name zeolite. There are numerous naturally occurring and synthetic zeolites, each with their own unique structure.

1.1.1 Zeolites

Zeolites are actually naturally occurring products. Not all naturally occurring zeolites have been recreated in the laboratory, and conversely, many zeolites have been synthesised that do not occur in nature.

Structurally, the zeolite is a crystalline aluminosilicate with a framework based on an extensive three-dimensional network of oxygen ions. Small dissolved silicate and aluminosilicate ions interact with structure directing agents eg organic cations and form organic-inorganic composites. So, situated within the tetrahedral sites formed by the oxygen can be either the Si^{4+} or an Ai^{3+} ion. The AlO_2^- tetrahedra in the structure determine the framework charge. This is balanced by cations that occupy nonframe-work positions. Ordered arrays are formed and with further condensation, this results in the growth of a 3D covalent crystalline network.

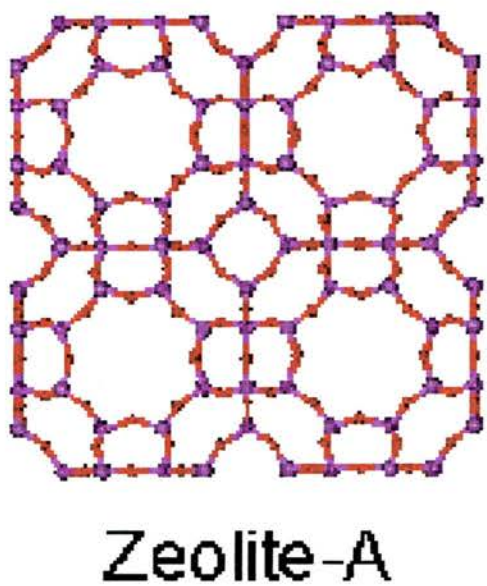

Figure 1. An example of a zeolite, Zeolite-A, used as a water softener in detergents. Purple = Si/Al, Red = O. No extra framework cations are shown.

A representative formula for a zeolite is written as:

$$\mathbf{M_{2/n}O \cdot Al_2O_3 \cdot xSiO_2 \cdot yH_2O}$$

M represents the exchangeable cations, generally from the I or II ions, although other metal, non-metal, and organic cations may also be used to balance the framework charge, and *n* represents the cation valence. These cations are present either during synthesis or through post-synthesis ion exchange. The value of *x* is equal to or greater than 2 because Al^{3+} does not occupy adjacent tetrahedral sites. The crystalline framework structure contains voids and channels of discrete size, unlike the microporous charcoal molecular sieves, a characteristic that separates them from the amorphous carbon molecular sieves.

1.1.2 Molecular sieve

A molecular sieve framework is based on an extensive three-dimensional network of oxygen ions containing generally tetrahedral-type sites. In addition to the Si^{4+} and Al^{3+} that compositionally define the zeolite molecular sieves, other cations are also able to occupy these sites. The cations are not necessarily isoelectronic with Si^{4+} or Al^{3+}, but are required to have the ability to occupy the framework sites. Cations such as Mg, Zn, Al, Si, Ge and Mn are known to fill these framework sites within molecular sieve structures.

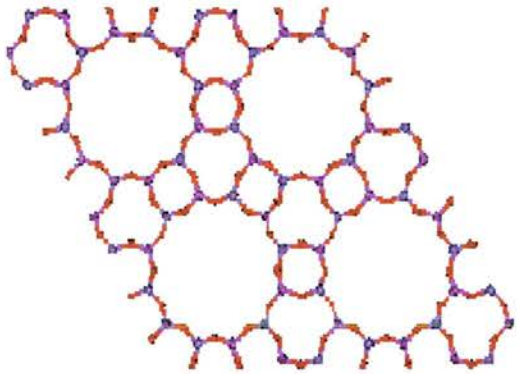

$AlPO_4$-5

Figure 2. An aluminiumphosphate molecular sieve
Purple = P/Al, Red = O. No extra framework cations are shown.

Zeolite molecular sieves have a net negative framework charge, however a molecular sieve does not need to display any charge over the framework. Molecular sieves, which contain only Si^{4+} in the tetrahedral sites, have a neutral framework. They exhibit properties such as hydrophobicity, to a large extent, although have no ion exchange capacity at all. The net charge on the $AlPO_4$ molecular sieves is also zero, which arises from AlO_2^- and PO_2^+ units existing in equal amounts in these structures. The $AlPO_4$'s have no ion exchange capacity either but do exhibit some attraction towards water, probably due to the polar nature of the Al-O-P bond within the structure.

Molecular sieve materials with compositions other than or in addition to silicon and aluminium, will collectively be considered under the more general category of molecular sieves.

MOLECULAR SIEVE	ZEOLITE
Microporous crystalline structure	Microporous crystalline structure
Variable elemental composition	Aluminosilicate
Variable framework charge	Anionic framework

Table 1. Differences between a molecular sieve and a zeolite

Molecular sieves containing pure silica are hydrophobic and can adsorb organic components from water, whereas molecular sieves comprising aluminosilicate frameworks are hydrophilic and can thus adsorb water from organic solvents.[3]

1.2 Zeolite Structures

The number of zeolite structures has been steadily increasing over the past 30 years, the total number recorded up to April 2003 is 139. This is due to the fact that the same framework structure can form many materials, which exhibit vast differences in their chemical properties. To distinguish each of the synthesised zeolites, each structure is given a 3-letter framework type code (FTC). An excellent example of a synthetic zeolite is the ACO[4] structure, figure 3.

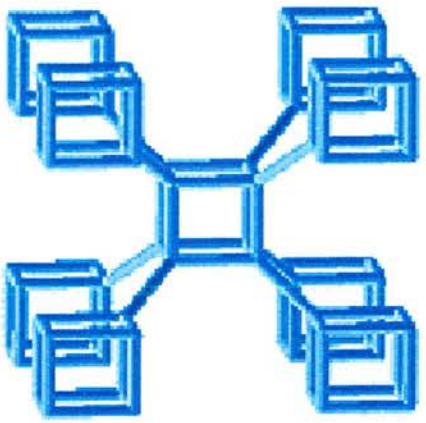

Figure 3. The synthetic ACO structure

It is built up from the cube double-four ring unit. One corner of one cube will link through another corner of a different cube, so it ends up with eight different separate cubes bonding onto the original one, through its eight corners. This is what this research is trying to achieve overall, producing microporous materials that are topologically similar to the ACO structure.

Another synthetic structure, which is of particular importance, is CLO, the gallophosphate cloverite[5], which has one of the largest ring pore openings of any of the synthesised framework architectures. It is a synthetic gallophosphate molecular sieve with a 20-tetrahedral-atom pore opening.

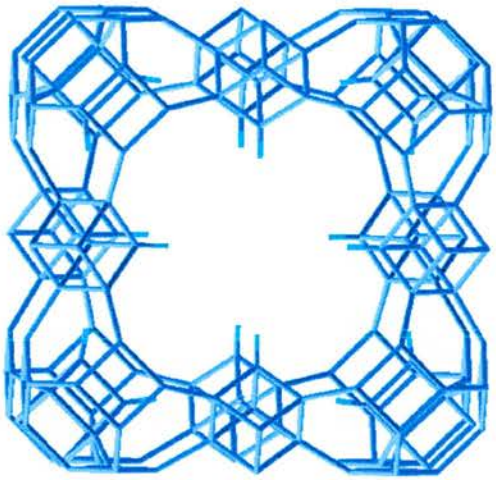

Figure 4. CLO: Cloverite structure

It has a cell volume of 17253.51 Å^3. The parameters of the cell are as follows; a=b=c= 25.840 Å and $\alpha=\beta=\gamma= 90.0^0$.

Before 1987 the largest zeolites had pore sizes below 10 angstroms. The pores of these zeolites contained only 12 oxygen atoms or fewer in the ring. However it was in 1987 that the Davis group[6] synthesised the aluminophosphate VPI-5, an 18-ring microporous material which had a 13 angstrom pore diameter. This was the first of many synthesised extra large pore zeolite-like materials.

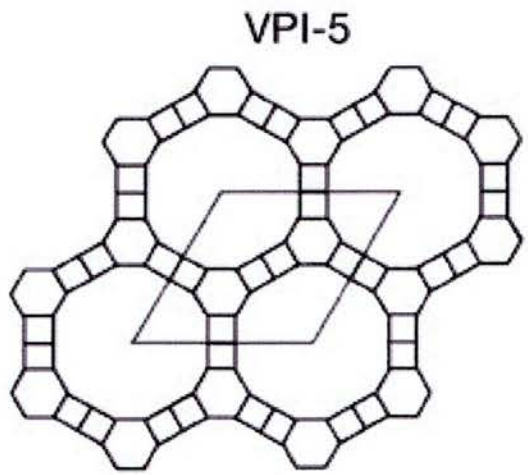

Figure 5. VPI-5 Aluminophosphate

10 years later the Davis group again produced another new material, CIT-5. The extra-large pore 14-ring zeolite had a diameter of just over 10 angstroms, the second extra-large pore zeolite discovered. This represented an important breakthrough in this particular field as the CIT-5 has the high thermal stability of a high silica-zeolite, but with the large pore size of VIP-5 and its successors.

Another advantage to this new material was that it did not require an organometallic SDA and the lengthy post-synthetic workup that follows.[7] The range of reactions over which zeolites can partake in shape selective analysis is a function of the zeolites pore size and its structure. Zeolites that have pore sizes of between 10 – 20 Å impact upon areas such as pharmaceuticals and the life sciences.[8]

1.3 The Phosphates

1.3.1 Aluminophosphates

The crystallised microporous materials can be divided into two main groups: zeolites (containing the framework Si, O and Al types)[9] and metallophosphates (eg aluminophosphates (Al, O, P)[10]. The phosphate group is of great interest, due to the wide diversity of the structures and pore openings that they present.[11]

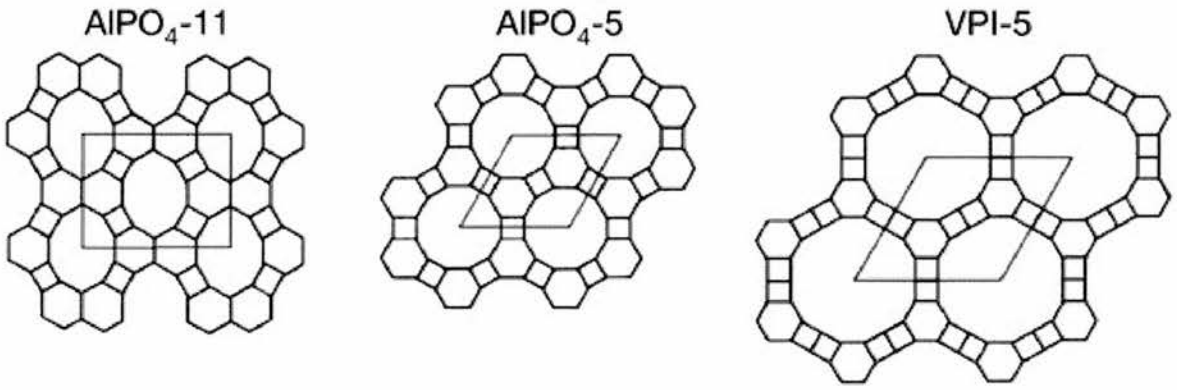

Figure 6. Aluminophosphates $AlPO_4$-11, $ALPO_4$-5 and VPI-5

These diagrams are representations of the pores. The line segments represent oxygen atoms that bridge between two tetrahedral atoms (intersection points) that are either Al^{3+} or P^{5+}, with alternation to give a composition of $AlPO_4$. The rhomboids indicate the unit cell.[3]

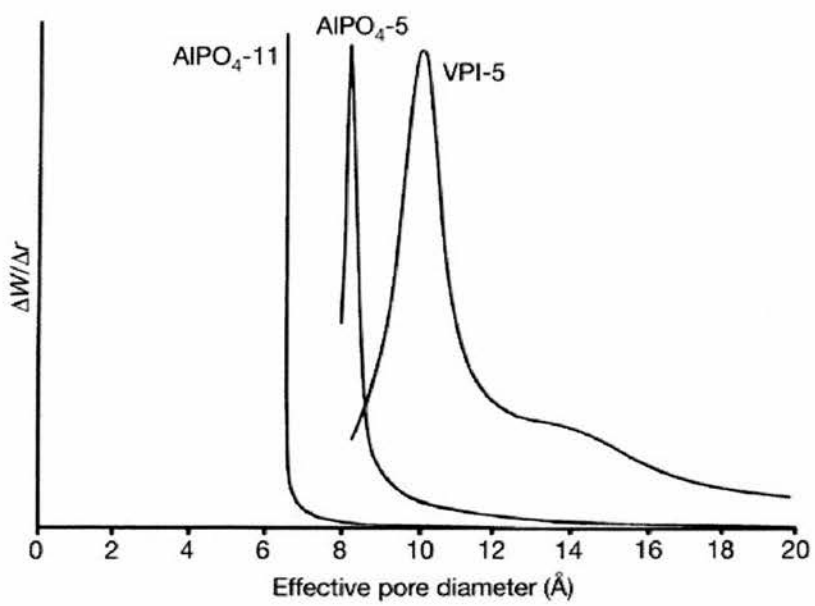

Figure 7. Graph showing the relative pore sizes of aluminophosphates including VPI-5

It was in the 1980's that the first microporous metallophosphates were discovered, along with the synthesis of the first aluminophosphates.[12] Initially it was the synthesis of the alumino-framework type, which garnered the most interest. Some of these

frameworks were analogues of the zeolite molecular sieves, and were designated $AlPO_4$-n, where the suffix *n* denotes a specific structure type. The synthesis of each framework is associated with a specific 'template' being added to the metallophosphate before it undergoes hydrothermal synthesis. The 'template' or structure-directing agent, SDA, is now typically an amine or organic molecule, which is thought to determine the overall geometry of the framework. It was discovered that when no SDA was added, no open framework structures were formed.[13] The aluminophosphate, $AlPO_4$-5, was one of the more exciting discoveries. Another metallophosphate synthesised with a similar composition is the zincophosphate, ZnPO-X. It is the structural analogue of important petrochemical catalyst, Zeolite Y or the Faujassite topology.[14] The incorporation of this element in the framework is extremely feasible, allowing for more novel frameworks to be produced.

1.3.2 Gallophosphates

It was in 1985 that the substitution of Al by Ga, allowed the first ever microporous gallophosphates to be synthesised.[15,16] This was an excellent breakthrough as gallium can adopt 4-, 5- as well as 6-coordination. Since then a large number of these gallophosphates were synthesised by the fluoride route[17,18], and it was widely believed that the fluoride ions played a major role by templating these gallium phosphate cubes.

The fluoride ion can display three different kinds of environments; it can bridge two gallium atoms in the gallophosphate framework and can be found as a terminal Ga-F group. Finally, it has a role stabilising the small structural units or the double four-rings.[19] One feature that was commonly found in the gallium phosphate species was the fluoride atom located at the centre of the D4R unit. However, it was discovered that it

was possible to synthesise a gallium phosphate cube which did not contain the fluoride atom at the centre.[20]

1.4 Uses of Zeolites and Microporous materials

Microporous solids such as the aluminosilicate zeolites and gallium phosphates are important materials, with applications in sensors, catalysis, ion exchange and gas separation.[21] Most recently they are being studied as host species for nanochemistry. The surfaces of the zeolites exhibit systematic ordered cavities, which act as pegboards for the regular array of nanomaterials in two dimensions.[22]

Zeolites were first used for organic synthesis in the 1960's.[23] ZSM-5, first synthesised in 1972 by Argauer and Landolt,[24] was applied to numerous refining and petrochemical processes with major success due to its unique shape selectivity. It is a medium pore (~6Å) zeolite with channels defined by ten-membered rings.

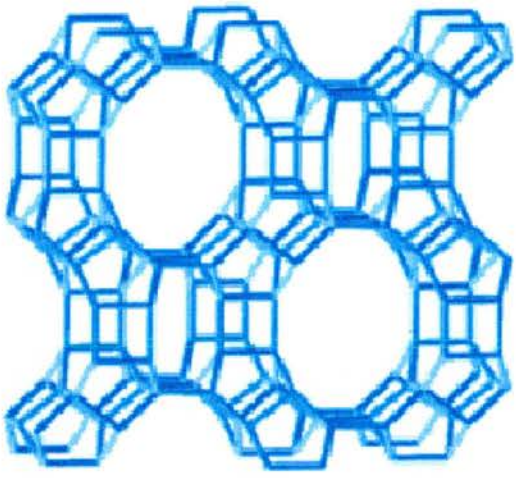

Figure 8. Zeolite Socony Mobil #5 ZSM-5

For instance, the monetary value of zeolites used in the petroleum cracking industry alone can be estimated at around 100 billion dollars today.[25]

1.4.1 Catalysis

Important reactions involving them as catalysts include hydrocarbon isomerisation and cracking syntheses[26], in which the zeolites interact well with organic molecules. These types of reactions involve catalysis by hydrogen-exchanged zeolites, whose protons bound in the framework give rise to very high acidity. They can also serve as reduction or oxidation catalysts, after metals have been introduced into the framework. Examples of this include titanium ZSM-5 in the production of caprolactam and copper zeolites in NO_x decomposition. The ZSM-5 zeolite has also been used as a membrane on a porous alumina tube, in the role of a drying agent.[27]

Their diversity enables them to produce a wide range of catalytic reactions including acid-based and metal induced reactions. The reactions take place within the pores and channels of the zeolites, which direct the overall structure formed by the end product,

figure 9. This is analogous to the 'Ship in a Bottle' idea, in which the synthesis is carried out in a porous zeolite (the bottle) to create the product (a ship).[28] The product could only be removed by breaking the bottle. But destroying the zeolite involved concentrated acids or bases, which could harm the product. However the first fully recyclable nanoporous material has been created whose organometallic open framework can be readily dissolved and built up using only mild reagents.[29]

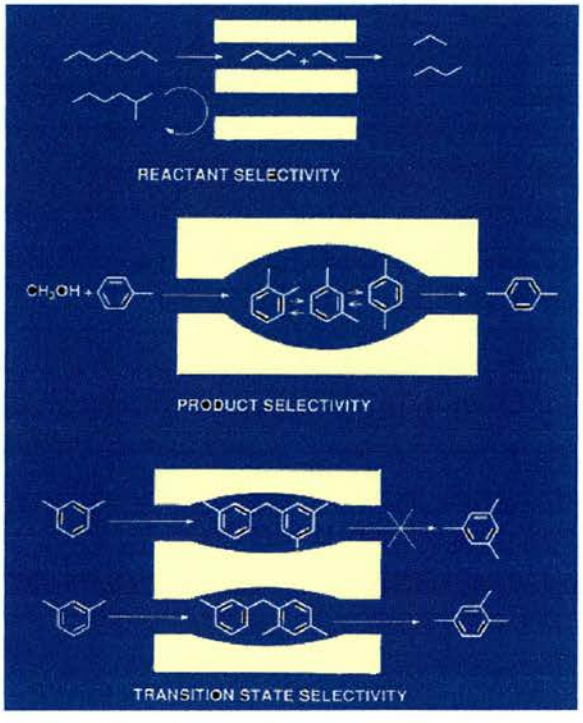

Figure 9. Reactant, Product and Transition state selectivity in industry.

Fine-tuning of the catalysts are essential for production of high-value chemicals, for use in pharmaceuticals and cosmetics.[13] These zeolites may also be re-usable, a significant advantage when used as catalysts in industry. Using relatively simple techniques such as heating to remove adsorbed organic molecules in the pores can regenerate them.[30]

1.4.2 Gas Separation

The ability to preferentially adsorb certain molecules, while excluding others, has opened up a wide range of molecular sieving applications. Sometimes it just depends on the size and shape of the pores to control access in and out of the zeolite.[31] In other cases different molecules can enter the zeolite, and while some can pass through the channels with relative ease, others can get stuck behind. An example of this is the purification of para-xylene by silicalite.[32]

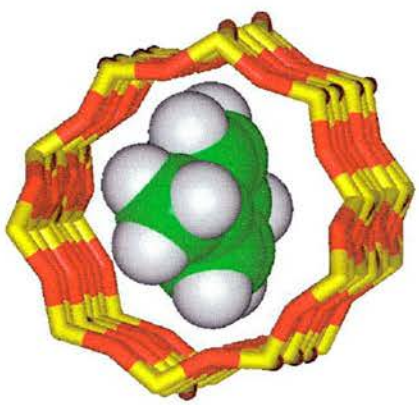

Figure 10. Purification of para-xylene by silicalite.

In this application known as gas separation, the zeolites act like sieves where the porous structure of the materials allows only molecules of a certain size to enter, figure 10. Varying the size and number of cations around the pores can attain fine-tuning of this process. Hence only the desired products can be synthesised in the cavities.

1.4.3 Ion Exchange

Finally in ion exchange, hydrated cations that are loosely bound to the zeolite framework can readily exchange with other cations when in aqueous media. Obvious applications of this process are in water softeners, replacing calcium ions with sodium

ions, and in detergents and soaps. Specific examples of this include removing radioactive ions from contaminated water, such as areas near to Chernobyl. In general zeolites and molecular sieves are being used at an increasing rate in a wide range of pollution control applications. They are used for odour control in waste materials and for removing unwanted effluent wastes from agricultural and industrial processes. The ZSM-5 ion-exchange catalyst is being used for the selective catalytic oxidation of ammonia to nitrogen.[33]

1.5 The Building Blocks

The utility of zeolites in industry depends significantly on their structural framework, so having the ability to control the overall architecture is an important goal in today's research. Being able to direct the architecture towards certain favourable structural units, by using these building units, is essentially the key.

Theories have been presented by O'Hare[19] and Férey[34] regarding microporous material formation. These materials are based on molecular building units or blocks, called pre-nucleation building units or PNBUs.[34] A building unit can be defined as the minimum assembly of atoms, ions or molecules which condense and give rise to the final solid, whatever the dimensions.

The building units (BUs) simply act as bricks and depending on their size, can determine the shape and size of the product. It can already be stated that many of the building units are polyhedral clusters. The BU can be the atom itself, the anionic

polyhedron around a metallic centre, or many polyhedra whether identical or different, linking together. These linkages can vary from weak to very strong.[34]

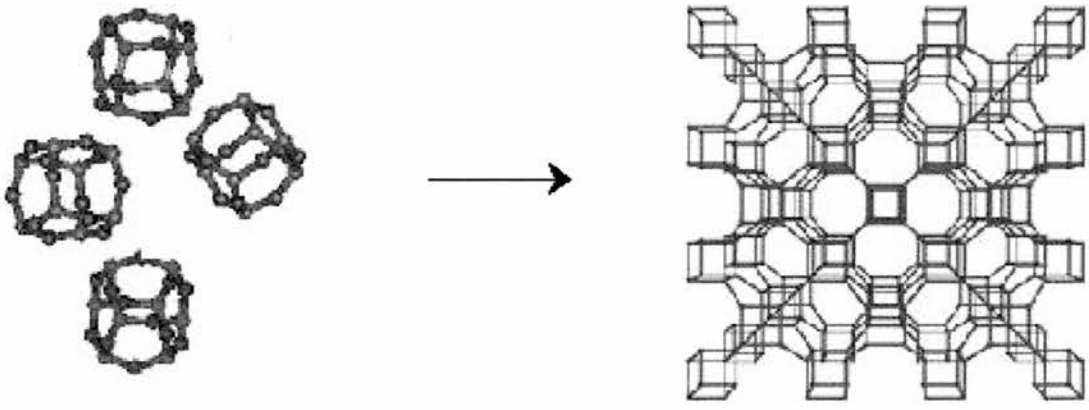

Figure 11. BUs: building up the framework – LEGO CHEMISTRY

These PNBUs are thought to be present in solution and condense either as they are or after undergoing small rearrangement/isomerisation reactions to form the resultant solid. They are also related to secondary building units (SBUs), depending on the geometric configurations of the primary building units. A few examples of these SBUs are shown in figure 12.

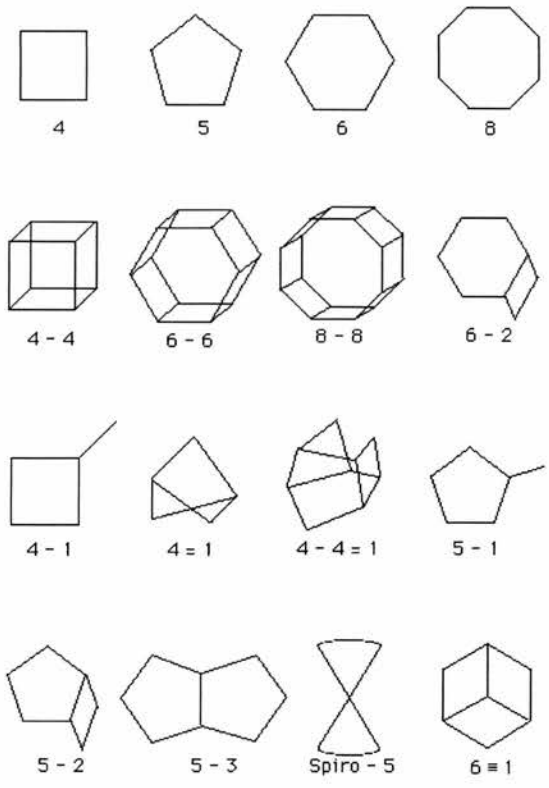

Figure 12. Secondary Building Units

The crystalline framework contains cages and channels of discrete size and 3-30 Å in diameter. The primary building unit of a molecular sieve is the individual tetrahedral unit. The topology of all known molecular sieve framework types can be described in terms of a finite number of specific combinations of tetrahedra called "secondary building units" (SBU's).[35] In Figure 12[36] the T atom belonging to a TO_4 tetrahedron is located at each corner, but the oxygens located near the mid-points of the lines joining each pair of T atoms are not shown. A molecular sieve framework is made up of one type of SBU only.[37]

These SBU's could either have the same structure as the PNBU's, or be fragments that are closely related to the PNBU's depending on whether or not rearrangement /isomerisation has occurred prior to, or during, condensation. This theory leads to a proposal that having control over the PNBU species present in solution should allow

some control over the architecture of the final resulting product. The solid microporous phases can be described in terms of these SBUs which are the building blocks for all of the known framework types. The topology of the final arrangement will result in the minimization of the lattice energy during the condensation of the building units or bricks.[2]

Building units are used as a way to describe the overall structure in terms of its bricks. It must be stated that they do not have to bear any resemblance to the synthesis mechanism. Increasing the size of the building unit also has its advantages. Cavities, which are created by the framework, increase significantly forming giant pores. Whereas before, with the usual solid-state inorganic frameworks, the cavities were very small and only able to accept the alkaline and/or alkaline-earth cations. Some examples of the gigantic pores, larger than the usual zeolites, originate from cages from zinc phosphates or hybrid organic-inorganic frameworks.[2]

1.6 The Double Four-Rings: D4Rs

Double-four rings are used as the starting materials in the synthesis of crystalline microporous materials, first introduced by Parise[13]. These double-four rings (D4Rs) are examples of pre-nucleation building units. In the concept for this type of research, the double-four rings are used as the building blocks for the structure. If you presuppose a structural unit, then this research is about trying to find extended structures that incorporate or wholly consist of the original starting unit. This is the type of theoretical chemistry that has previously been studied by Férey.[36] A D4R unit, see figure 13, is

made of eight corner-sharing tetrahedra MO_4 (M=metal), commonly found in existing inorganic structures such as the previously mentioned alumino- or gallophosphates.

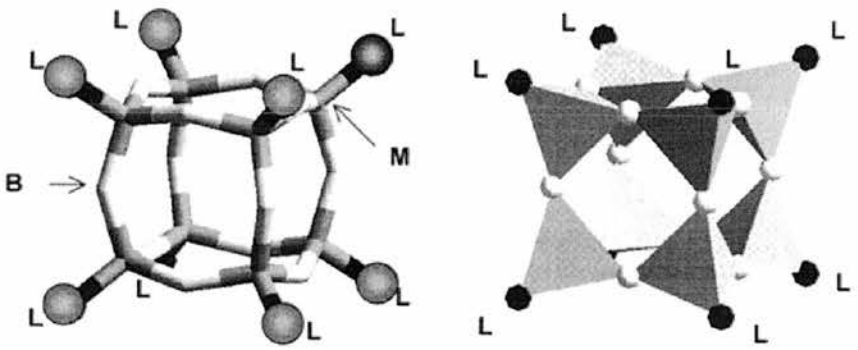

Figure 13. Cylinder (left) and Polyhedral (right) representation of the D4R unit. L=Ligand atom, B=Bridging atom, M=Metal atom

The bridging atoms in these examples are oxygen. Other known inorganic structures containing only D4R units include arrangements where the D4Rs are in chains, see figure 14, Mu-3, or in sheets of D4R units, ULM-18, again figure 14.[36]

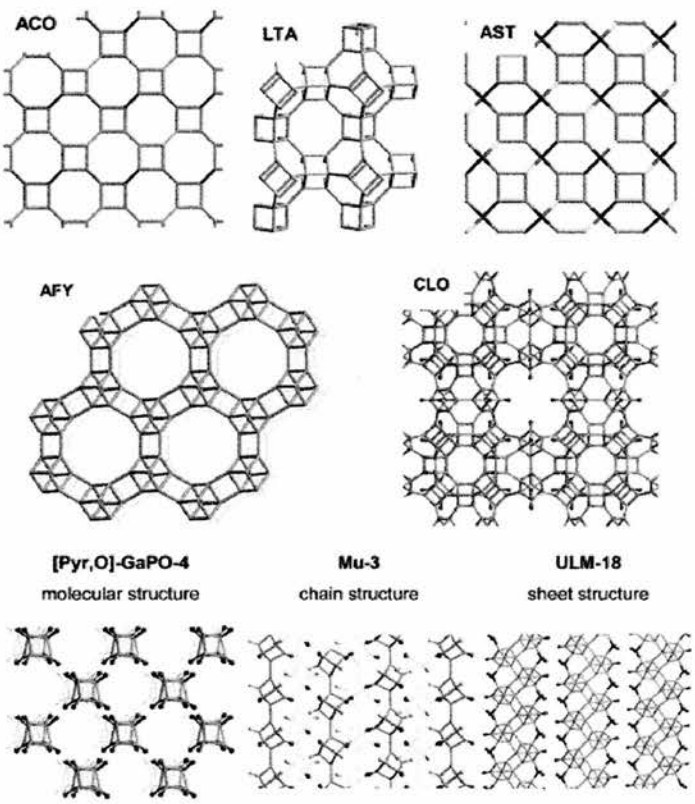

Figure 14. Existing inorganic structures containing double-four ring units.

It was previously thought that fluorine was required as a structure-directing agent to form the D4R unit.[35] However recent studies have shown that [pyr,O]GaPO-4[36] possesses occluded oxygens instead of fluorines, which leads to the theory that fluorine is no longer necessary to form the D4R unit. Also, a limited number of known existing zeotypes made exclusively of D4R units include the previously mentioned ACO and – CLO topologies. The AST zeotype, figure 14, requires these units plus other supplementary tetrahedral species to generate the framework.

These D4R units are important because of their rigid three-dimensional shape. The D4Rs which are studied in this project, include the gallophosphate analogue which has oxygen occluded at the centre[37], and the germanate analogue with fluoride occluded at

the centre instead of oxygen. The last example is the tetramethylammonium silica based cube[38], which has the approach of using quaternary ammonium salts as the structure-directing agents.

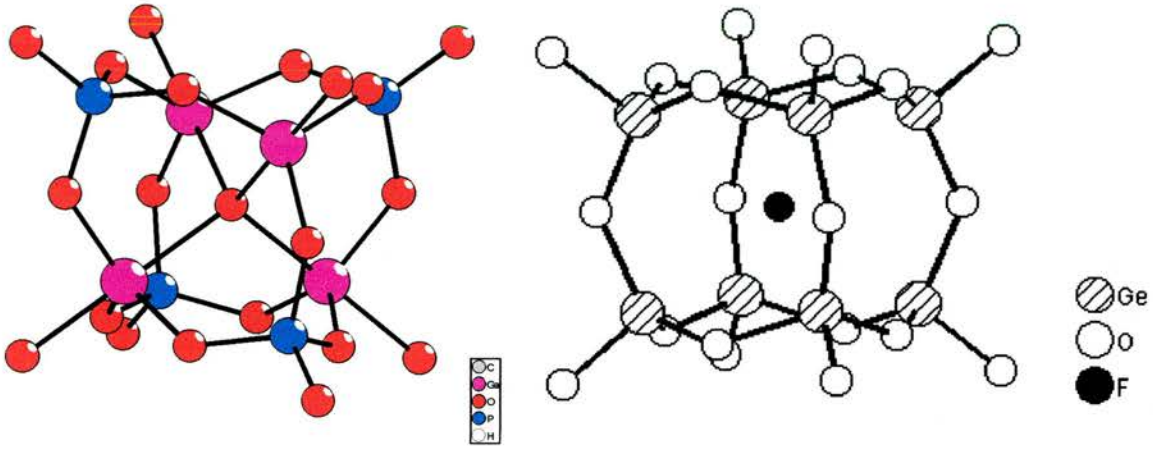

Figure 15. The Ga, and Ge based D4Rs

In the Ga cube, the oxygens (red) are situated at the centre of each 'edge', the phosphorous (blue) is at four of the 'corners' and the gallium (pink) is found at the other four corners of the 'cube'. An oxygen is also found at the centre of the cube. However in the germanate analogue, the fluoride ion (black), is occluded at the centre with eight germanium ions positioned at the eight 'corners' of the cube. The oxygens (white) are again situated at the centre of each 'edge'.

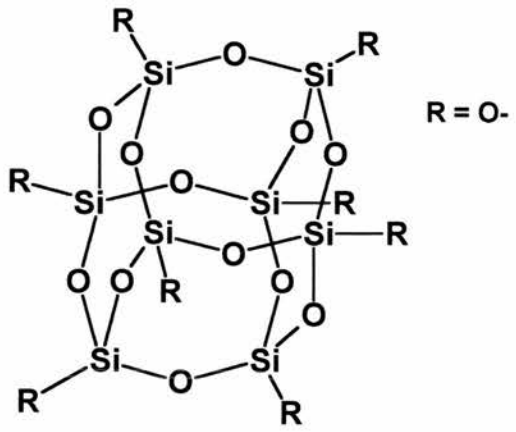

Figure 16. The Silica based D4R

Figure 16 shows the Silica based cube with Si at the 'corners'. The oxygens again are located along the 'edges', bonded between two silicons.

1.7 Synthesis

Making zeolites and microporous solids is quite a delicate and precision accurate process. However if all goes well, an ordered crystalline structure will be the end result. The conditions under which the hydrothermal synthesis takes place have not changed much since the days of Barrer[39] and Milton[40] in the 1950's.

In general, the reagents are added together and mixed thoroughly to allow a homogeneous solution or gel to form. Organic chemicals called the structure-directing agents are added to steer the self-assembly of the microporous solid in a desired direction. The mixture is then placed in a teflon-lined autoclave and placed in an oven at the required temperature.

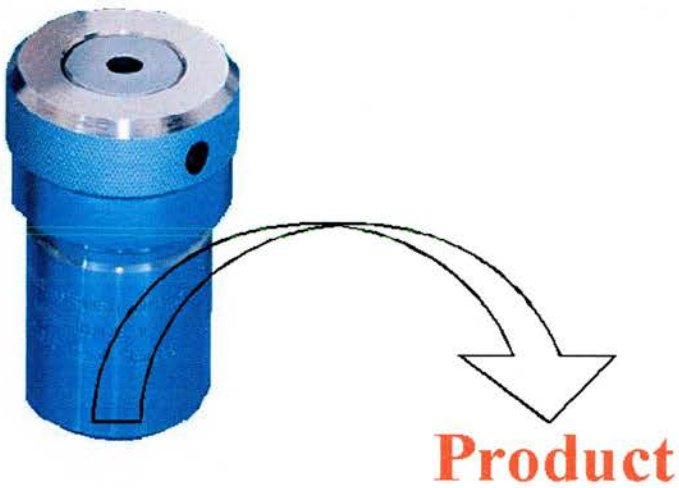

Figure 17. Teflon-lined autoclave

Conditions such as temperature, time and pH can be altered in order to synthesise various products. The temperatures involved in these reactions range from 90 ^{0}C up to 250 ^{0}C, but above this the temperature is ineffective in producing decent results. Extended reaction time at high temperature and/or high pressure usually results in dense phases. Other variables include the framework cations such as Si^{4+} and Al^{3+}, the concentrations of the solutions and the actual structure-directing agent. The solvent for each hydrothermal synthesis can also play an important part in the overall framework architecture. Every avenue is being explored in the synthesis of these microporous materials. Working at the molecular level, small differences can make a big difference in selectivity. In fact this type of synthesis and how the actual microporous material forms is not understood as well as the dot and arrow schemes of normal organic synthesis mechanisms.

1.7 References:

1) A.F. Cronstedt, *Adak. Handl. Stockholm*, 1756, **17**, 120

2) R. Szostak, *Molecular Sieves: Principals of Synthesis and Indentification*, Van Nostrand Reinhold, New York, 1989, Ch.1

3) Mark E. Davis *Nature*, **417**, 813-821, 2002

4) See the International Zeolite Association website (www.iza-online.org)

5) W. M. Meier and D. H. Olson, Atlas of Zeolite Structure Types, 3rd ed., Butterworths, 1992.

6) W. M. Meier and D. H. Olson, Atlas of Zeolite Structure Types, 3rd ed., Butterworths, 1992.

7) Wagner, P; Yoshikawa, M; Lovallo M; Tsuji, K; Tsapatsis, M; Davis, M.E; *Chem. Comm.*, 1997, 2179

8) Freyhardt, CC; Tsapatsis, M; Lobo, RF; Balkus, KJ; Davis, ME; *Nature*, 1996, **381**, 295

9) P. Feng, X. Bu, G.D. Stucky, *Nature*, 1997, **388**. 735

10) S. Oliver, A. Kuperman and G.A. Ozin, *Angew. Chem. Int. Ed.* 1998, **37**, 46

11) A. Matijasic, V. Gramlich, J. Patarin, *J. Mater. Chem.*, 2001, **11**, 2553

12) W.H. Baur, R.X. Fischer, *J. Chem. Soc., Dalton Trans.*, 2002, 630

13) J. B. Parise, *J. Chem. Soc., Chem. Comm.*, 1984. 1449

14) A. Simon-Masseron, J. Paillaud, J. Patarin, *Chem. Mater.*, **4**, 1000-1005, 2003

15) A. Matijasic, J-L. Paillaud, J. Patarin, *J. Mater. Chem.* 2000, **10**, 1345

16) T. Azais, C. Bonhomme, L. Bonhomme-Curry, *J. Chem, Soc., Dalton Trans.*, 2002, 609

17) M. Wiebcke and D. Hoebbel, *J. Chem, Soc., Dalton Trans.*, 1992, 2451

18) P. Reinert, B. Marler and J. Patarin, *Chem. Comm.* 1998, 1769

19) D.S. Wragg, R.E. Morris, *J. Am. Chem. Soc.*, 2000, **122**, 11246

20) R.J. Francis and D. O'Hare, *J. Chem. Soc., Dalton Trans.*, 1998, **120**, 6822

21) Daniel Maspoch, Daniel Ruiz-Molina, Klaus Wurst et al. *Nature Materials*, **2**, 190-195, 2003

22) Sasaki M et al., *Micropor. Mesopor. Mater*, **21**, 597-606, 1998

23) Davis, ME; Saldarriaga, C; Montes, C; Garces, J; Crowder, C; *Nature*, 1998, **331**, 698

24) R.J Argauer, G.R. Landolt, United States Patent 3,702,886 (1972), assigned to Mobil Oil

25) http://www.zeolyst.com/html/faq.html#two

26) Coma V, Pergher S.B, Maesen Th.L.M, Buglass J.G, *Nature*, **396**, 353-356 (1998)

27) Tao Sun, *Nature,* **389,** 704-706, 1997.

28) Hongbin Zhao, Tetsuro Jin, Koji Kuraoka, Tetsuo Yazawa, Chem. Comm, 2000, 1621-1622

29) Lubomira Tosheva, Valentin Valtcher, Johan Sterte, *J. Mater. Chem.*, 2000, 2330-2337

30) Jing Li et al., *Angwe. Chem. Int. Edn.*, **42**, 542-546; 2003

31) http://www.bza.org

32) http://www.ch.ic.ac.uk/vchemlib/course/zeolite/applications.html

33) Richard Q. Long, Ralph T. Yang, Chem. Comm., 2000, 1681-1682

34) G. Férey, *J. Sol. State Chem.* 2000, **152**, 37

35) W. M. Meier, Molecular Sieves, Society for Chemical Industry, London, 10 (1968).

36) Ch. Baerlocher, W. M. Meier and D. H. Olsen, Atlas of Zeolite Framework Types, Elsevier Amsterdam, 2001, 5th Edition.

37) G. Férey, *J. Am. Chem. Soc.*, 2002, **124**, 15326-15335

38) I. Hasegawa, S. Motojima, *J. Organo. Chem.*, 1992, **441**, 373.

39) R.M. Barrer, The Hydrothermal Chemistry of Zeolites, Academic Press, London, 1982, 1st Edn

40) D.W.Breck, W.G. Eversole, R. M. Milton, T.B Reed and T.L.Thomas, *J. Am.Chem. Soc.*, 1956, **23**, 5963.

2.0 AIMS

2.1 Synthesis of microporous materials using D4Rs

The main aim of this research project was to synthesise microporous materials, which contained in their structure definite crystalline architectures. These materials would then be analysed by the appropriate experimental techniques, such as powder X-Ray diffraction, single crystal diffraction and by a synchrotron radiation source.

The first step towards achieving this is to synthesis the molecular building blocks, which were chosen for this part of the project. The double four-ring unit or D4Rs are the gallium based cube, the silica based cube and the germanate analogue. These molecular D4R analogues would be used as the starting materials for the synthesis of microporous crystalline structures under hydrothermal conditions. Key factors for getting results include changing the times of the incubation period, as well as the temperatures under which the mixtures in the autoclaves are placed, from 90 - 200 ^{0}C. One of the most important aims would be to add different reagents to the starting materials in the hope of gaining effective linking on a molecular level.

2.2 Linking the D4Rs

The D4R units are important due to their rigid three-dimensional shape, which should ensure some order in the resulting product. As well as the starting material and the solvent to form the homogeneous gel, a structure-directing agent is required to try and steer the assembly of the microporous solid in the desired direction.

The first idea was to try and link the cubes using 2+ ions, specifically Zn^{2+} ions. The compound chosen was zinc chloride, $ZnCl_2$. Reactions at room temperature and in the oven, under more extreme hydrothermal conditions, should accompany refluxes in order for more complete and accurate results to be achieved. Refluxing temperatures would be up to 80 ^{0}C, whereas autoclave temperatures range from 130 - 190 ^{0}C.

The proposed equation for the reaction is:

$$TMA_8Q_8 + 4ZnCl_2 \rightarrow Zn_4Q_{8(s)} + 8TMACl_{(aq)}$$

TMA_8Q_8 = the silica based cube

Figure 18 shows how the Zn could theoretically link the cubes together in the final crystalline solid, giving the ordered structure.

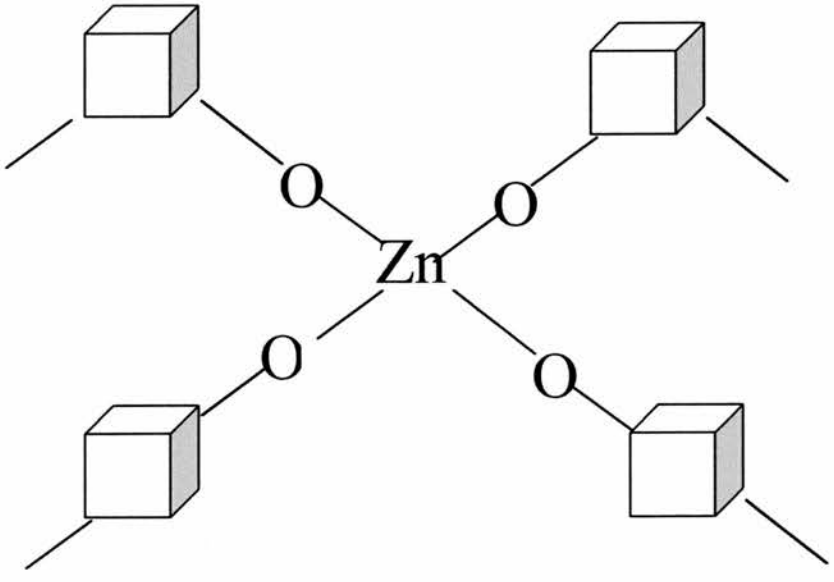

Figure 18. Possible linking of Zn with the Si cubes – analogous to the AST structure shown in chapter 1.

The Zn^{2+} cation could link with the oxygens, through four different corner ions of four different cubes. This pattern would repeat itself throughout the structure, giving a degree of order.

Another method, which is quite similar, is to use the mercury ion, Hg^{2+}, in the form of mercury chloride. The only difference is that the mercury ion would in theory, coordinate through only two of the oxygens which are bonded to the silicate ions at the corners of the cubes. So in effect this should give a more linear and hence a different crystalline structure than the zinc.[1]

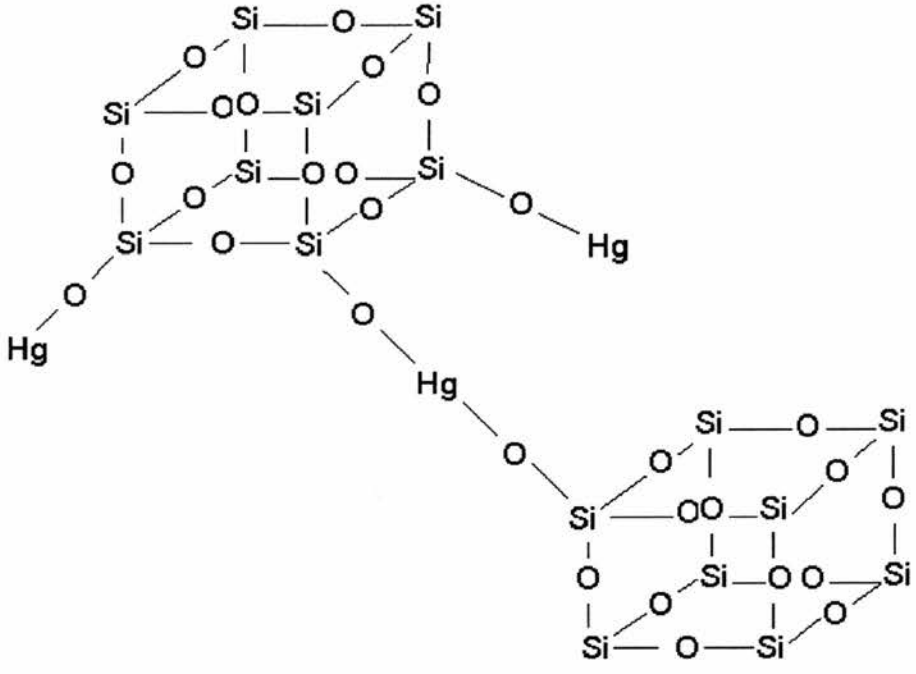

Figure 19. shows mercury linking the cubes

The next logical step would be to introduce other mercury compounds, such as mercury sulphate, oxide and nitrate.

2.3 Using other 2+ ions

In keeping with the idea of using metal ions to link the cubes together, metals from group II – the alkaline earth metals, and the transition metals were chosen for the next experimental stage. Again these reactions would be carried out at room temperature and in the bombs under specific hydrothermal conditions.

Examples of these metal ions which could prove useful are barium, copper, calcium, and zinc, particlularly in the form of the nitrates. Monovalent Ag^{+} ions would also be included. Two other compounds, dipyridinium dihydrochloride and imidazole hydrochloride would also be used in these type of reactions. The increased rigidity in these chemical compounds should help to give a more linear molecular chain incorporating the cubes.

2.4 Cyclam: 1,4,8,11-Tetraazacyclotetradecane

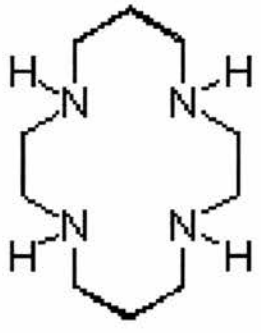

Figure 20. Cyclam: 1,4,8,11-Tetraazacyclotetradecane

The macrocycle cyclam has been known for decades and the complexation chemistry in which it is so heavily involved has been studied extensively. Such macrocyclic ligands

can lead to complexes with enhanced thermodynamic and kinetic stability, compared to open-chain analogues[2]. The metal ions such as Cu^{2+} or Zn^{2+}, when added to the cyclam ring, can bond to the four nitrogens.

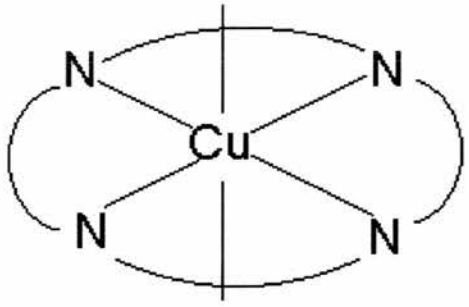

Figure 21. Cu binding in the cyclam ring

This leaves two free vertical bonding sites above and below the plane of the copper-nitrogen ring, allowing the $GaPO_4$ cubes to bond onto the copper, giving uniform ordered crystallinity in the structure.[3]

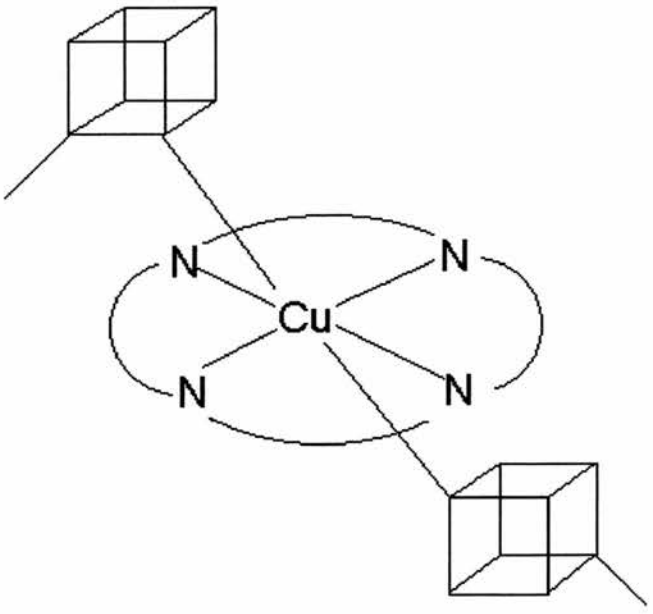

Figure 22. $GaPO_4$ cubes bonding to Cu in the cyclam ring.

The research for this project will involve many reactions with the cubes incorporating differing solvents, temperatures and structure directing agents. This should yield interesting results for the synthesis of microporous solids.

2.5 References:

1) M. Kaupp, H. G. von Schnering, *Inorg. Chem.*, 1994, **33**(12); 2555-2564.

2) A.E. Goeta, J.A.K. Howard, D. Maffeo, H. Puschmann, J.A.G. Williams and D.S. Yufit, *J. Chem. Soc., Dalton Trans.,* 2000, 1880

3) D. S. Wragg, G. B. Hix and R.E Morris, *J. Am. Chem. Soc.* **120**, 6822-6823, 1998

3.0 EXPERIMENTAL TECHNIQUES

3.1 Hydrothermal synthesis

Microporous material synthesis is usually the crystallisation of a stirred mixture or solution at high temperature: hydrothermal synthesis. Once the reactants have been added together in a teflon-lined autoclave, the mixture is stirred to produce a homogeneous gel, which is sealed in a bomb and heated for a few days at the required temperature. The product is recovered by filtration, washed by cold solvents and finally dried.

It is often difficult to reproduce the exact material obtained from one experiment to the next, as there are many variables that play a major role in the crystallisation process. For example pH, acidity, framework cations, solvent, structure directing agent, time, temperature and the actual isomerisation and rearrangement that takes place during the synthesis, all factor into what will hopefully crystallise as a microporous material.

3.2 X-Ray Diffraction

It was in 1912 that Max Von Laue[1] successfully recorded the first X-ray diffraction pattern.

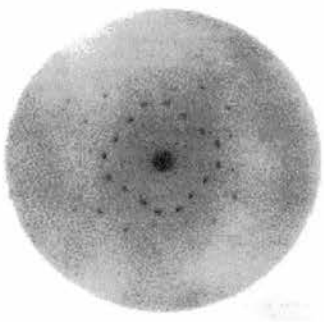

Figure 23. X-rays scattered by $CuSO_4$ crystal.

Figure 23 shows the first ever scatter process to be achieved; the X-rays are scattered into a characteristic pattern by a copper sulphate crystal. The phenomenon of X-ray diffraction occurs when atomic planes of a crystal cause an incident beam of X-rays to interfere with one another as they leave the crystal. This will happen if the wavelength is approximately the same magnitude as the interatomic distance between the planes.

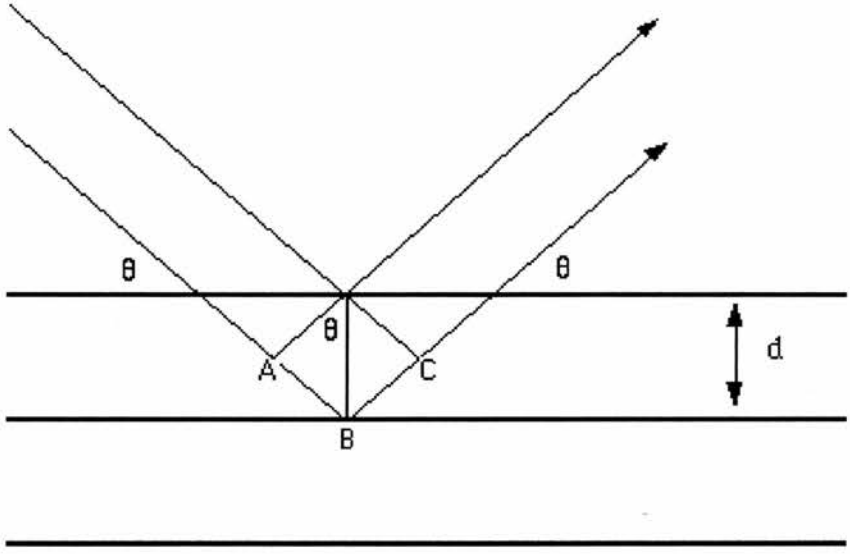

Figure 24. Bragg's Law – X-rays reflecting from a crystal surface

Diffraction will occur if Bragg's Law[2] is satisfied. Bragg's Law describes the mechanism by which X-ray diffraction occurs and explains the patterns generated by the reflected rays. If a beam of coherent light is incident on a plane of regularly spaced atoms at a certain angle, some will interact with the atoms and some rays will get scattered in all directions.

Two English physicists Sir W. H. Bragg and his son Sir W. L. Bragg derived Bragg's law in 1913, which refers to a simple equation:

$$n\lambda = 2d\sin\theta \quad (3.1)$$

It explains why crystals reflect X-ray beams at certain angles of incidence theta, θ, the angle between the beam and the lattice plane. As shown in figure 24, the variable d is the distance between the atomic layers in a crystal, while the variable λ, is the wavelength of the incident X-ray beam. The integer is n. The lower beam has to travel a further distance of what is equivalent to AB + BC in figure 24, and is known as the path difference. This extra distance must be an integral (n) multiple of the wavelength (λ) for the phases of the two beams to be the same and for maximum positive interference to occur. It is commonly known as X-ray diffraction, XRD. As X-rays penetrate deep into the crystal, lattice planes will reflect the incident beam. Constructive interference is produced if equation 3.1 is satisfied; however if not, then the result is destructive interference. The lattice planes are referred to as Miller Indices which are vector representations for the orientation of an atomic plane in a crystal lattice. They are defined as the reciprocals of the fractional intercepts which the plane makes with the crystallographic axes. These are represented by three integers, (*hkl*). These Miller planes correspond to planes of atoms in the crystal lattice. The X-rays are scattered by the electrons which surround the nuclei of the atoms, and this is what produces the diffraction pattern. The positions of the spots indicate the unit cell and the intensities show where the atoms are. The symmetry of the diffraction pattern relates to the crystal symmetry and space group.

The diffraction pattern is the Fourier transform (FT) of the electron density within the unit cell. The structure factor, $\underline{F}$, is a vector which is proportional to the intensity, and consists of the amplitude and phase. However, the phase of each reflection is unknown

and this is the phase problem. In order for the accurate representation of the electron density to be given, the phase is required. Direct methods attempts to solve this problem by attempting to derive the phases using this equation:

$$\sin(hkl) \times \sin(h'k'l') = \sin(h+h', k+k', l+l') \quad (3.2)$$

It relies on the fact that the amplitude and phase of a structure factor are related through electron density. It works better the stronger the reflections are. Once the phases are known, the refinement of the structural model can begin by using the Least Squares technique.

Least squares refines the model by finding the remaining atoms which provide the best possible agreement between the diffraction pattern calculated by the Fourier transforms and the observed one. Since the phases are not observed the comparisons are drawn entirely on the amplitudes, $|F_o|$ and $|F_c|$ for observed and calculated amplitudes respectively. Least-squares defines the 'best-fit' of two sets of data as shown in equation 3.3.

$$\Sigma w(F_0^2 - F_c^2) \quad (3.3)$$

It has the same idea as fitting a 'best-fit' line through a set of points, except that there are more variables. The atomic coordinates, atomic displacement parameters and the site occupancy are some of the factors that are refined.

3.2.1 Single Crystal X-Ray Diffraction

Much of the work carried out in the laboratory nowadays can be analysed by the single-crystal x-ray diffraction technique. This is because of modern computers, which can evaluate the millions of calculations required to solve a structure in a few seconds. Also area detectors can record many reflections at the same time which means a faster data set collection. Once the crystal has been mounted and centred in the path of the beam, the collection of data can begin.

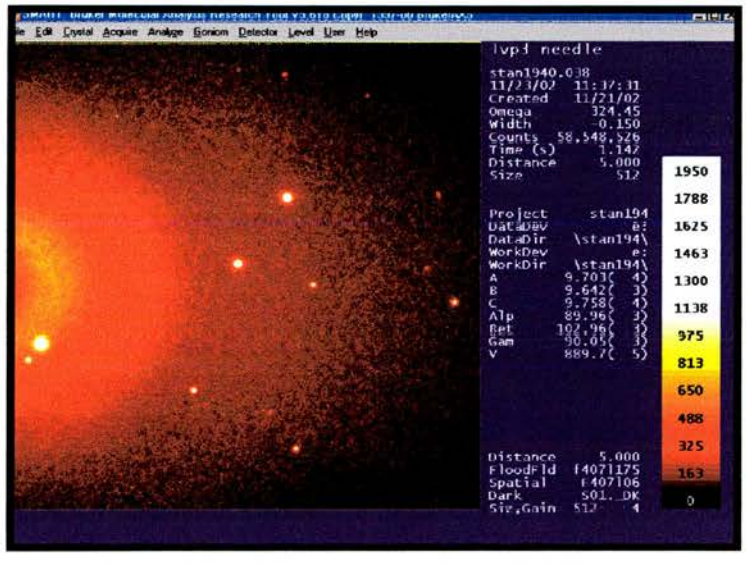

Figure 25. Pattern from single crystal x-ray diffraction

A diffractometer, which has an area detector, can collect a complete dataset in less than a day. Whereas traditional diffractometers use point detectors, which measure the intensity of each diffracted beam individually in sequence, an area detector records the diffraction pattern over a large area of reciprocal space simultaneously. The image is then stored digitally as a 'frame' of diffracted intensity information. Many frames are collected in turn, as the crystal is rotated in a series of small steps. The frames are then analysed, and the intensity of each individual 'reflection' can be determined.[3] The X-ray source is either Mo or Cu, with wavelengths of 0.705nm and 1.540nm respectively.

A major advantage that the single crystal technique has over powder diffraction is that in principle, you can learn everything there is to know about the structure. However, it also has its disadvantages. When preparing the sample for diffraction, it is a time-consuming and difficult task to mount and orientate the crystal. Also, if more than one phase is present, it can be difficult to realise that there is more than one set of reflections. Some of the crystals produced from hydrothermal synthesis were too small, typically 30 x 30 x 10μm, to be characterised by the in-house single crystal diffraction technique. Diffraction data was collected using high-flux synchrotron radiation.

3.2.2 Powder X-Ray Diffraction

It can be difficult to produce crystals suitable for single crystal x-ray diffraction, so the powder diffraction technique is used. It helps with phase identification purposes and is useful for confirming the identity of a solid material by determining its crystallinity and phase purity, then solving the structure. In the powder, the sample consists of many small crystallites with random orientations. Modern powder x-ray diffractometers consist of an x-ray source, a movable sample platform and a detector for the rays. Using the same x-ray source as single crystal diffraction, the x-ray beam is passed through the randomly-orientated microcrystals to produce a pattern of rings on a screen.

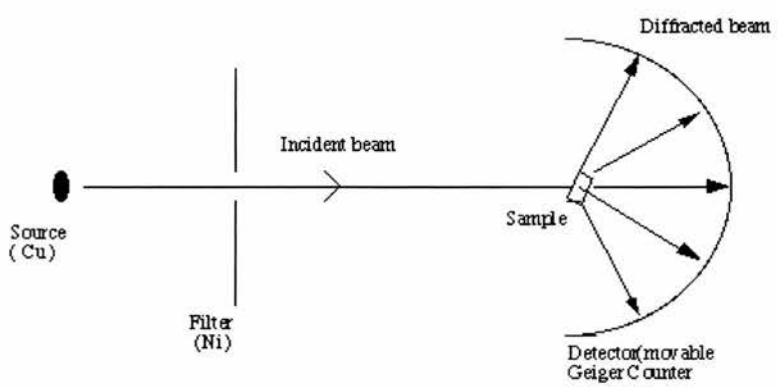

Figure 26. Schematic of an X-Ray Powder Diffractometer

The sample holder will spin slowly to reduce heating, and to ensure that all possible crystalline orientations are in the beam. The powder should be ground up to create a uniform particle size, ensuring all crystallite orientations are present in the sample. The one major disadvantage to this technique is that it provides less information than single-crystal diffraction, however it is simpler and faster.

Results were collected on:

- a Phillips Xpert diffractometer which operates on reflection geometry and uses Cu K_{α} radiation. It also has a secondary beam monochromator, which is used to reduce the effects of fluorescence.

- a STOE STADIP diffractometer operating in transmission mode. It uses monochromated Cu $K_{\alpha 1}$ radiation and is equipped with a primary beam monochromator. The STOE can either take 0.5mm quartz capillaries or discs with the prepared samples.

3.3 Synchrotron Radiation

Synchrotron radiation is an extremely intense, polarised, powerful technique used to collect ultra-fast high resolution crystal data.[4] Electrons generate the X-rays as they are accelerated through electromagnetic fields, which are situated at various points around the storage ring, SRS.

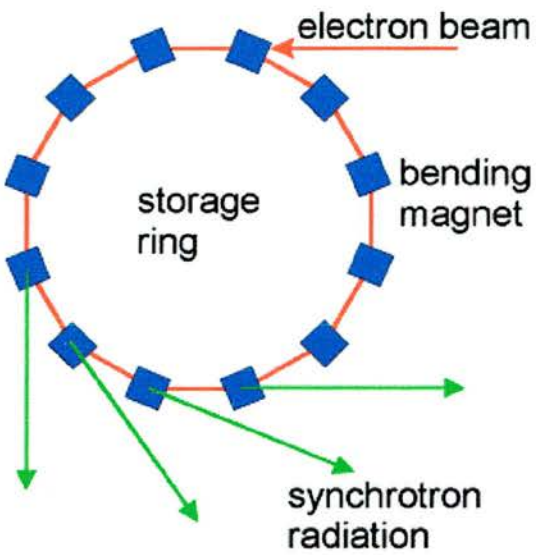

Figure 27. Synchrotron Storage Ring

Figure 27 shows an illustrated diagram of a storage ring.[5] The electrons are accelerated, injected into the ring and held at a fixed energy by a constant magnetic field. The synchrotron radiation is emitted tangentially from the beam in the ring. However, the electron current of the ring needs to be replenished every 12-24 hours, as the electrons are scattered out of the beam due to interactions. Stations placed strategically around the storage ring can collect the emitted radiation as it passes through bending magnets, monochromators and detectors.

The CCLRC Daresbury Laboratory Synchrotron Radiation Source[6] is situated in Cheshire in the UK and station 9.8 was used for the single crystal x-ray diffraction. The station can receive up to 3.8mrads of beam, which is focused in the horizontal plane by the asymmetrically cut triangular silicon monochromator, cooled by a GaInSn alloy. The (111) monochromator has an asymmetric cut of 2.01^0, which gives an optimum focus at the sample for a wavelength of 0.7 Å. The station is equipped with a Bruker AXS SMART CCD area detector diffractometer on which the high-flux single-crystal diffraction was carried out. The wavelength required for our samples was 0.68 Å.

Figure 28. Bruker AXS SMART CCD area diffractometer at station 9.8, Daresbury.

As the crystals were too small to be mounted on an in-house diffractometer, a two-stage fibre was required for use at station 9.8. This consists of 1-2mm piece of glass wool glued to ~5mm glass fibre attached to a pip. The crystal could then be mounted on the end of the glass wool by epoxy resin or viscous oil.

3.4 References:

1) Friedrich, W., Knipping, P. & von Laue, M. *Sber. Bayer. Akad. Wiss.* **303** (1912).

2) W. H. Bragg and W. L. Bragg, *X-rays and Crystal Structure*, G. Bell and Sons, London, 1924, Ch.2

3) http://www.eserc.stonybrook.edu/ProjectJava/Bragg/

4) P. Coppens, Synchrotron Radiation Crystallography, Academic Press, London, 1992

5) Synchrotron Chemical Crystallography, W. Clegg, *J. Chem. Soc., Dalton Trans.*, 2000, 3223-3232

6) http://www.srs.ac.uk/srs/

4.0 Experimental

4.1 Preparation of the cubes

The term cube is only used as a point of reference for the D4Rs; at this time the structures of these microporous solids are not known for definite, so the term 'cube' is given in order to help define the synthesised materials, see figure 29.[1]

The first set of experiments were the syntheses of the starting materials, the double four-rings or the D4Rs:

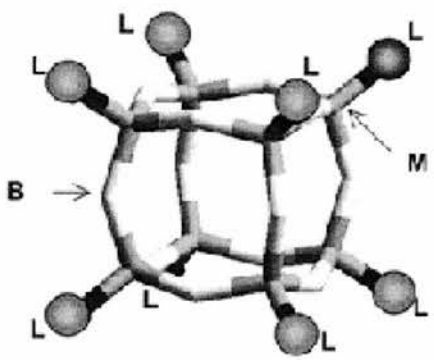

Figure 29. Cylinder representation of the D4R unit
L=Ligand atom, B=Bridging atom, M=Metal atom

The three D4R starting material units are as follows:

- Tetramethylammonium Silica 'cube'
- Gallium Phosphate, $GaPO_4$ 'cube'
- Germanate 'cube'

4.1.1 Tetramethylammonium Silica 'cube':

Tetraethoxysilicate (4.48 mls) was added to a 2.0M tetramethylammonium hydroxide pentahydrate solution in methanol (10 mls).[2] H_2O (1.8 mls) was also added whilst stirring vigorously. Further methanol was introduced into the reaction vessel to bring the total volume of methanol to 20 mls. Stirring was maintained for 24 hours. After this time the solution was concentrated and placed below room temperature in the fridge to recrystallise out overnight. The Si-based crystals produced were washed with cold water and dried, and characterised by single crystal X-ray diffraction.

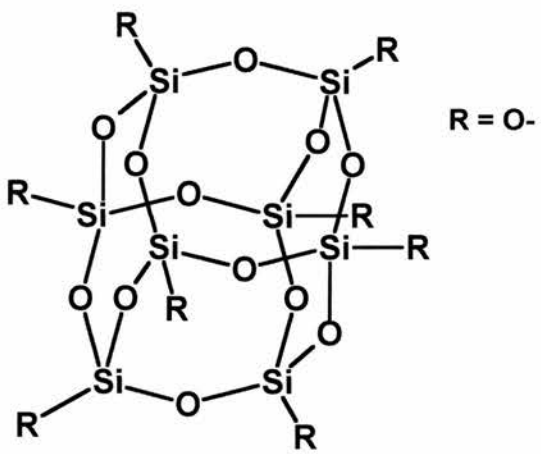

Figure 30. The TMA Silica based 'cube'

4.1.2 Gallium Phosphate cube:

Gallium sulphate, $Ga_2(SO_4)_3$ (2.5 g), was ground up until fine, and then 0.5 g was placed in each of the five sample bottles. H_2O (2ml) was added next, with H_3PO_4 (0.3 g). The pyridine (8 mls) was weighed out separately in the fume cupboard for each sample, then quickly added to avoid spillage. Each mixture was stirred for 1 hour to ensure that the $Ga_2(SO_4)_3$ fine particles were well dispersed, after which the pH was taken. The solutions were transferred to Teflon lined autoclaves and placed in a 150 ^{0}C

oven for two days.[3] After this time the samples were removed. Filtered with water and acetone (80%:20%) respectively) and then dried.

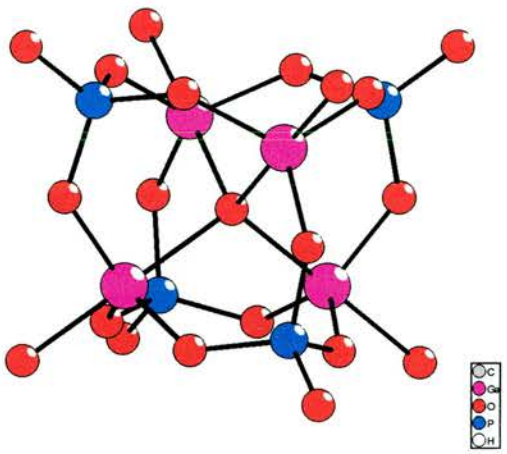

Figure 31. The Gallium 'cube'

4.1.3 Germanate cube:

Germanium dioxide (3.61 g) was dissolved in 50.31 g of a solution that had 3.43 x 10^{-4} mols of TEMAOH per gram. H_2O (49.40 g) was removed by rotary evaporator, then hydrofluoric acid (HF 48%, 0.72 g) was added and stirred by hand. The mixture was placed in the autoclave and put in a 150 ^{0}C oven for eight days, after which time the resulting product was washed with cold methanol and dried.

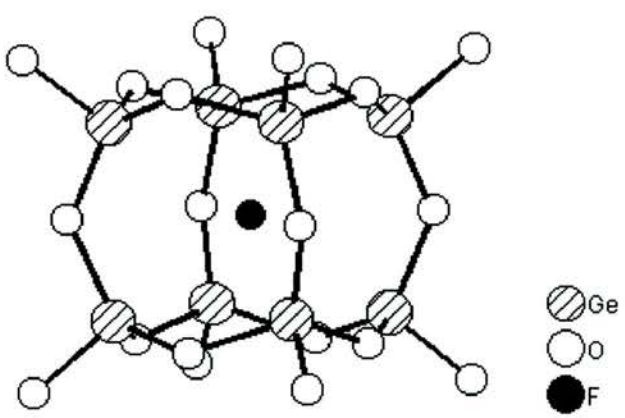

Figure 32. The Germanium 'cube'

Once the Si-, Ga-, and Ge- based cubes were synthesised; they were used as the basis for the next set of reactions.

4.2 Variations on the synthesis:

It is the unknown effect of temperature and time on these pre-nucleation building units in solution that we wish to investigate. Bombs were prepared which contained the chemicals required for the synthesis of the gallium cube. Instead of being heated for two days at 150 ^{O}C, two of the three bombs were removed from this temperature and placed in 170 ^{O}C and 190 ^{O}C ovens respectively, for a certain length of time. The idea of this experiment was to try and show what would happen if the 'cube' formed in solution, immediately followed by being placed in a hotter environment. This was to encourage the condensation of the cubes. To be able to compare results, the bomb that was left in the 150 ^{O}C oven would be used as the standard, so the three bombs were simultaneously reacting under three different environmental conditions. They were all left in for the exact same length of time. Once filtered, washed through with H_2O and dried, x-ray powder patterns were made of each of the three samples. See the results section, 5.0.

4.3 TMA silica-based cube experiments

As well as working with the silica-based cubes under hydrothermal conditions in the bombs, a different approach was also taken. Being more soluble, we can involve the silica-based 'cubes' in low temperature experiments.

First attempt:

The TMA-Si cube (2 g), $ZnCl_2$ (1.612 g) and H_2O (50 mls) were added to a reaction vessel, which was maintained under reflux for five hours at 100 ^{0}C. The resulting product was filtered and dried.

Second attempt:

This time the TMA-Si cube and the $ZnCl_2$, same amounts, were each dissolved separately in H_2O (25 mls). Once dissolved, the solutions were added together and again put under reflux at 100 ^{0}C for five hours. Again the product obtained was filtered and dried.

The last two experiments involved trying to work with the silica based cube at room temperature and not under excessive high temperatures for long periods of time. However, this would also be required. The TMA-Si cube (0.5 g) was added to H_2O (6 mls) and $ZnCl_2$ (0.403 g). The mixture was continuously stirred for an hour before being placed in a teflon lined autoclave and put in a 190 ^{0}C oven for three days. Various other combinations of the TMA-Si cube were experimented with, including $ZnCl_2$ with the bombs in the ovens and the products of the refluxing experiments.

4.4 Incorporating $HgCl_2$ - Mercuric Chloride

Using Mercuric Chloride was the next logical step to take in working with the cubes. In the zinc chloride the zinc had a charge of 2+, which would mean it could be co-ordinated to the four corners of the TMA Si-based cube. So to try and improve on the results so far, a mercury compound was introduced. Instead of linking to four corners of

four different TMA-Si cubes, the mercury, which also has a charge of 2+, will only link to two corners of two different cubes. Hence it should be linear, producing a more ordered structure. The ratio of mols of TMA-Si cube to mols $HgCl_2$ is 1:4. Again, as with the previous experiments involving $ZnCl_2$, the $HgCl_2$ was refluxed with the 'cube' as well as being placed in the bombs in the oven.

Refluxing with $HgCl_2$:

The TMA Si-cube (2 g) was dissolved in H_2O (25 mls) and added to $HgCl_2$ (0.32 g), which had also been dissolved in the same volume of H_2O. The two solutions were mixed together and refluxed for four hours. After which time the product was filtered and dried.

In the bomb:

The TMA-Si cube (1 g) was dissolved in H_2O (8 mls). $HgCl_2$ (0.16 g) was added to the solution and stirred for one hour. It was then placed in a 190 ^{0}C oven for three days. The product was filtered with H_2O and dried.

4.5 Experimenting with other mercury compounds:

The other mercury compounds, which were used, were:

- Mercuric Oxide - HgO
- Mercuric Nitrate - $Hg(NO_2)_2$
- Mercuric Sulphate - $HgSO_4$

The Silica based cube (3 x 0.5 g) was placed in three autoclaves, which each contained HgO (0.24 g), $Hg(NO_2)_2$ (0.287 g) and $HgSO_4$ (0.293 g) respectively. H_2O (10 mls) was added to the autoclaves and each was stirred for one hour. The homogenised solutions were then put into the oven at 150 ^{0}C for three days. Again the products were filtered and dried.

Several reactions were carried out involving the Mercury compounds. This included changing the times and temperatures of the hydrothermal synthesis for each bomb. The solvents were also altered, from H_2O to CH_3OH and $(CH_3)_2CHOH$. However the only real conclusive results came from the reactions which incorporated $HgCl_2$ with the silica based cube under hydrothermal synthesis.

4.6 Experiments involving Group II ions

Another approach for this type of synthesis was to use metals from group 2 and the transition metals, such as barium, copper, silver, zinc, calcium, dipyridine dihydrochloride and imidazole hydrochloride. These last 2 compounds in particular would hopefully give a more linearly linked structure with the cubes.

These reactions were left at room temperature for two weeks instead of being placed in the bombs under hydrothermal conditions. Each reaction was set up separately in a 250ml conical flask and covered to prevent evaporation from occurring.

Metal ion compound (g)		TMA-Si cube (g)	H_2O (mls) –solvent
$Ba(NO_3)_2$	0.4590	0.5	40
$AgNO_3$	0.4076	0.5	40
$Ca(NO_3)_2$	0.2884	0.5	40
Dipy	0.4025	0.5	40
$Zn(CH_3CO_2)_2$	0.3858	0.5	40

Table 2. Alkaline earth and Transition metal compounds with TMA-Si cube

The mole ratio in all of these experiments was calculated at:

Metal ion **1**: TMA-Si cube **4**

The values in the table reiterate this.

No immediate product was formed in the conical flasks which contained the dipy and the zinc acetate compounds. However, it was noted that a solid gel-like mass was produced almost instantaneously in the $Ba(NO_3)_2$ reaction vessel. For the remaining metal compounds, calcium nitrate and silver nitrate, yellow and black gel-like products were formed respectively, after the two-week time period. After washing with cold acetone and drying, the white powders retrieved showed that no significant results had been achieved.

So after this first set of experiments, it was decided to try and change the solvent in the reactions, as the silica-based cube dissolves slightly better in methanol than water. Again the reactions were set up at room temperature for the same length of time, fourteen days.

Reacting compound (g)		**TMA-Si cube (g)**	**Solvent (mls)**	
Dipy	0.4025	0.50	Methanol	40
Dipy	0.4025	0.50	Isopropanol	40

Table 3. Dipyridine dihydrochloride with TMA-Si cube using different solvents

White gel-like products were recovered for these two reactions, in fact for all of the above seven experiments no crystalline products were formed. Each solution was filtered, washed with cold acetone and dried.

The filtrates of each sample were retained since no suitable crystalline results were collected. Evaporation, which was allowed to take place slowly with these samples at room temperature, yielded interesting results. After another two-week period, long needle shaped crystals began to form from both of the dipy filtrate solutions. The solvents for each of these were methanol and isopropanol. These were the first set of results to come from those particular experiments. However, for the rest of the filtrates, no suitable products were formed.

To try and get around the problem and stop it from happening, it was decided to try these two methods:

- Diluting – diluting the solutions of the CH_3OH/silica based cube and/or the dipy/solvent, would decrease the concentrations of the reacting mixture, hence slowing down the reaction rate.

- Pipetting – another way to slow the reaction down is by adding the dipy/solvent solution through a pipette.

These experiments were continued under these conditions at room temperature for quite some time. Through trial and error, it appeared that the temperature was not high enough for any significant kind of reaction to occur. Other compounds such as copper nitrate, zinc nitrate and zinc chloride had also been tried with the cubes, along with the imidazole hydrochloride compound.

Reacting compound (g)		**TMA-Si cube (g)**	**Solvent- CH_3OH (mls)**
$C_3H_4N_2.HCl$	0.011	0.03	25
$Cu(NO_3)_2$	0.025	0.03	25
$CoSO_4$	0.029	0.03	25
$ZnCl_2$	0.014	0.03	25

Table 4. Reactions involving the cube

Using another method to try and slow down the reaction, this one involved dissolving the dipy or metal ion compound in a solvent such as H_2O (5 mls), which was then placed in a small vial. The silica-based cube, dissolved in CH_3OH (5 mls), was placed in a similar flask. Both vials were then put in a larger container, which was filled with CH_3OH (10 mls) to the same level as the top of the vials. This would allow very slow dispersion to take place between the two solutions, stopping the product from crashing out too quickly. The container was then sealed to prevent evaporation from taking place. These reactions were left for six weeks.

4.7 Reactions at higher temperatures

Since the synthesis at room temperature was proving futile, these reactions would have to take place at higher temperatures. Using the same moles ratio as before, 4:1 for the metal compound to the cube, respectively. The experiment would be carried out the same as before, only this time the solutions would be stirred for one hour to produce a homogenised mixture. They were then placed in a teflon-lined autoclave and put in a 150 ^{0}C oven for length of time. All of the metal compounds, which had been experimented with previously, were again used for these sets of experiments.

Reacting compound (g)		TMA-Si cube (g)	Solvent (mls)		Time (days)
$C_3H_4N_2.HCl$	0.011	0.03	$(CH_3)_2CHOH$	8	9
$C_3H_4N_2.HCl$	0.011	0.03	CH_3OH	8	6
$Cu(NO_3)_2$	0.025	0.03	$(CH_3)_2CHOH$	8	9
$Cu(NO_3)_2$	0.025	0.03	CH_3OH	8	6
$CoSO_4$	0.029	0.03	CH_3OH	8	6
$ZnCl_2$	0.014	0.03	CH_3OH	8	6

Table 5. Compounds under hydrothermal synthesis

The table shows just some of the many reactions carried out, involving the reacting agents and the 'cubes'. The temperatures ranged from 130 ^{0}C to 190 ^{0}C, and would be used as a starting point. Because this type of synthesis is difficult to predict, at this stage it is basically trial and error with the bombs in the oven. The autoclaves were put under hydrothermal synthesis for a couple of days, or left in for a couple of weeks at a time.

4.8 The Gallium Phosphate cubes

The preparation of the gallium cubes, as described above in 4.1.2, is relatively short as it only takes two days at 150 ^{0}C. To investigate this further, the autoclaves containing the gallium cube standard, were left under these conditions for differing lengths of time.

The question could be asked; how would long term hydrothermal synthesis affect the already crystallised gallium cubes?

Autoclaves, which had been under 150 ^{0}C for two days, were transferred and placed under temperatures of 170 ^{0}C and 190 ^{0}C respectively. Three other autoclaves were left in the 150 ^{0}C oven as standards for comparison. At random intervals, every two to six weeks, an autoclave was removed from a specific temperature, was filtered, washed and dried. The time period over which this experiment was conducted was five months.

The $GaPO_4$ cube was also reacted with imidazole hydrochloride, $Cu(NO_3)_2$, and $Zn(NO_3)_2$. Table 6 shows only some of the hydrothermal reactions which took place.

Reacting compound (g)		**$GaPO_4$ cube (g)**	**Solvent (mls)**		**Time (days)**	**Temp ^{0}C**
$C_3H_4N_2$.HCl	0.011	0.10	H_2O	8	14	90
$Cu(NO_3)_2$	0.013	0.05	H_2O	8	6	150
$Zn(NO_3)_2$	0.015	0.092	H_2O	8	14	90

Table 6. Reactions of the $GaPO_4$ cube under hydrothermal synthesis

4.9 The Introduction of Cyclam

As described in the aims section, the idea to introduce to cyclam, 1-4-8-11-Tetraazacyclotetradecane to the cubes, was to try and incorporate their structure onto the cyclam ring. A host metal ion would bond onto the nitrogens in the ring as well

bonding with the cubes in the vertical and horizontal axial positions above and below the ring, see figure 22.

The first set of reactions, carried out at room temperature, involved $Cu(NO_3)_2.3H_2O$ and CH_3OH as the solvent. Cyclam (0.20 g) was dissolved in CH_3OH (75 mls), with $Cu(NO_3)_2.3H_2O$ (0.240 g) being added to the solution. It was kept at room temperature for one hour, after which time the TMA-Si cube (0.11 g) was added while stirring. A purple precipitate formed after one hour of stirring. The solvent was allowed to evaporate off slowly over five days, leaving the crystalline product. The experiment was also repeated using $ZnCl_2$ and $CuSO_4$. Reactions with the $GaPO_4$ cube and the cyclam were also carried out with the same metal compounds as mentioned above. The solvent used was either H_2O or methanol. These bench reactions did not give any suitable findings, so more experiments were conducted in the bombs and autoclaves at higher temperatures.

Compound (g)		**$GaPO_4$ (g)**	**TMA–Si (g)**	**Cyclam (g)**	**Solvent (mls)**		**Time (days)**	**Temp (^{0}C)**
$Cu(NO_3)_2$	0.012	0.092	----	0.010	H_2O	8	14	90
$Zn(NO_2)_3$	0.015	0.093	----	0.010	H_2O	8	14	90
Dipy	0.020	----	0.100	0.010	CH_3OH	8	14	90
$C_3H_4N_2.HCl$	0.009	----	0.100	0.010	CH_3OH	8	14	90

Table 7. Metal compounds with Cyclam under hydrothermal synthesis

Variations on the hydrothermal synthesis, in the autoclaves, include imidazole hydrochloride and dipyridine dihydrochloride with the $GaPO_4$ cube in H_2O, CH_3OH and isopropanol. Also using cyclam at these temperatures with the silica based cube and the $GaPO_4$ cube. Autoclaves were placed under temperatures as low as 90 ^0C for a lengthy period of time, two weeks as opposed to two days, see table 7.

4.9.1 References:

1) G. Férey, *J. Am. Chem. Soc.*, 2002, **124**, 15326-15335

2) A. Provatas, M. Luft, Jun C. Mu, A. White, *J. Organo. Chem.*, 1998, **565**, 159.

3) D.S. Wragg, R.E. Morris, *J. Am. Chem. Soc.*, 2000, **122**, 11246

5.0 Results and Conclusions

5.1 Introduction: Synthesising the starting materials

X-ray diffraction patterns were collected every time the starting materials of the gallium or silicon cubes had been synthesised. They were compared to previously obtained patterns of the materials. If the peak positions were in correlation with the original patterns, then the samples would be used in the continuing experiments. An example is shown in the appendix section 7.0, figure 50, the powder pattern of the synthesised gallium cube.

The possible outcomes for these types of reactions include various rearrangement and isomerisation reactions taking place, some desirable and others not so desirable. Once the double-four rings or D4R's are synthesised, it is interesting to see what happens to these starting materials when under hydrothermal synthesis.

The possible outcomes include:

a) The D4Rs linking together in a desired manner to produce a crystalline ordered structure. The cubes would bond through all eight 'corners' to eight separate other cubes, hence forming large ring opening pores and channels running through the solid.

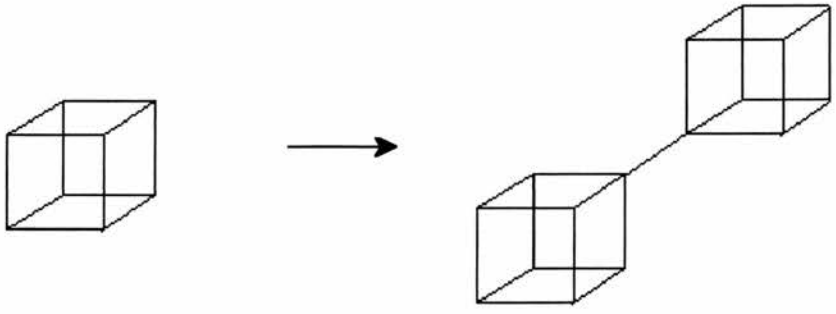

b) The D4Rs breaking up completely. The cubes could rearrange themselves completely, breaking up into smaller fragments such as chains and square units, instead of remaining intact as the D4R's.

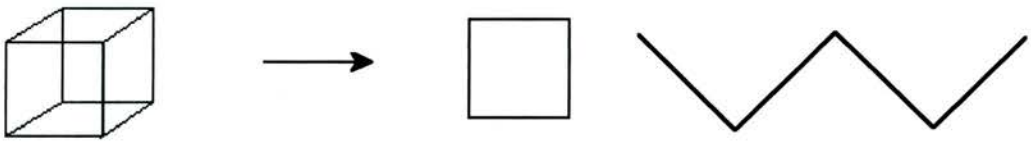

c) The D4Rs only partially breaking up in solution. The cubes can separate, with fragments disconnecting from the original cube. The resulting architecture would not contain any double-four ring units.

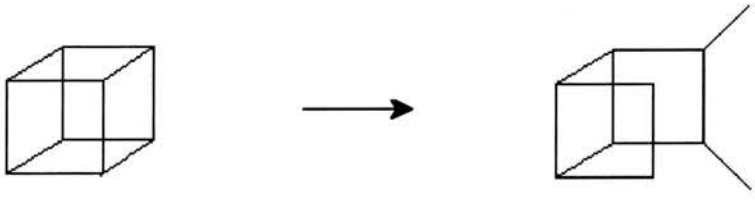

The difficulty with this synthesis is trying to avoid the undesirable breakups within the structure of the cube as a whole. It is extremely difficult to judge at what point the cubes can disintegrate and break up, and it is this fine line that is being investigated. Ideally, for this process, we want the cubes to remain intact in solution, then while undergoing synthesis, to bond together in such a way so as to form ordered crystalline microporous solids. Trying to get the cubes to bond linearly will be a particular target for this research, and hopefully adding structure-directing agents will aid in the synthesis.

Producing any crystalline material will be a good result, as a lot of the time gels tend to precipitate out too quickly. However, under higher temperatures we will be able to eliminate this problem. The first approach was simple: to see what occurred when the starting materials were placed under high temperatures for a prolonged period of time.

5.2 $GaPO_4$ cube under hydrothermal synthesis at high Temperature

Do the D4Rs condense at high temperatures intact? This is the question that we will now be trying to answer. Autoclaves containing $Ga_2(SO_4)_3$, pyridine, H_2O and H_3PO_4 were placed under hydrothermal synthesis at 150 ^{0}C for three days. A standard was kept at this temperature for a further three days, while two other autoclaves, having been removed from the 150 ^{0}C oven were placed under temperatures of 170 ^{0}C and 190 ^{0}C respectively. All of the autoclaves were kept under these temperatures for a further four days. Once cooled, washed and dried, x-ray powder patterns were collected for each of the samples. The products collected from the autoclaves were white crystalline solids.

5.2.1 Powder X-ray Diffraction

Powder patterns showed that the positions of the peaks altered significantly between each sample. The crystalline materials subjected to the higher temperatures, produced patterns whose peaks were situated further towards the left on the 2θ axis. In the 170 ^{0}C sample the lowest peak was found at approximately 10^0, whereas for the 190 ^{0}C sample, its lowest peak came at approximately 8^0 on the pattern. Positions of the peaks on these graphs relate to the size of the unit cells, a large unit cell can correlate to a large pore size. Braggs law, equation 5.1, shows how to calculate the unit cell:

$$n\lambda = 2d\sin\theta \quad (5.1)$$

where d is the spacing between the crystal planes:

$$d_{100} = \text{unit cell}$$

If λ remains constant and unit cell spacing d increases, then angle $\sin\theta$ must decrease, and peaks on the graph must move further down to the left. So a large unit cell has peaks at the smallest 2θ angle values. So it was clear that something was happening at the higher temperatures, in the 190 ^{0}C sample. Possibly the cubes were undergoing rearrangement and breaking up. Under the microscope, it could be clearly seen that two different crystal types had formed:

- long thin monoclinic crystals
- rhomboidal crystals.

The next step was to take the crystal sample, known as lvp3, to Daresbury for further detailed analysis.

5.2.2 Synchrotron Radiation

The Synchrotron radiation source at Daresbury could give a more enhanced picture of the structure of the crystals, which were too small to be used on the in-house diffractometers in St.Andrews. Diffraction data was collected on a Bruker AXS SMART CCD area-detector diffractometer on the high-flux single-crystal diffraction station 9.8 at CCLRC Daresbury Laboratory Synchrotron Radiation Source, Cheshire, UK. Data

reduction and cell refinements were carried out using Bruker SAINT packages. Structures were solved by direct methods (SHELXS-97) and refined with the full-matrix least squares technique (SHELXL-97) using WinGX. All non-hydrogen atoms were refined anisotropically and hydrogen atoms were geometrically placed. Details of the data collected and the structure parameters are given in the tables for each structure.

5.2.3 Monoclinic crystal

Gallium phosphate with pyridine, H_2O and phosphoric acid at 150 ^{0}C for two days, then 190 ^{0}C for three days, produced two crystal types: monoclinic and rhomboidal. These are the results for the monoclinic crystal: lvp3n.

Identification code	**Stan194/lvp3n**
Empirical formula	C_{20} H_{24} Ga_{12} N_4 O_{52} P_{12}
Formula weight	2360.71
Temperature	150(2) K
Wavelength	0.69320 Å
Crystal system, space group	Monoclinic, $P2_1/n$
Unit cell dimensions	a =8.9050(4) Å α =90^0
	b =17.9333(8) Å β =107.923(2)^0
	c =9.0925(4) Å γ =90^0
Volume	381.57(11) Å^3
Z, Calculated density	1, 2837 Kg/m^3
Absorption coefficient	6.234 mm^{-1}
F(000)	1140
Crystal size	0.06 x 0.06 x 0.06 mm
Theta range for data collection	2.22 to 27.55^0
Limiting indices	-11<=h<=4, -21<=k<=23, -11<=l<=12
Reflections collected / unique	7356 / 3401 [R(int) = 0.0334]
Completeness to theta=27.55	99.0%
Absorption correction	None
Refinement method	Full-matrix least-squares on F^2
Data / restraints / Parameters	3401 / 0 / 232
Goodness-of-fit on F^2	1.066
Final R indices [I>2sigma(I)]	R1 = 0.0328, wR2 = 0.0879
R indices (all data)	R1 = 0.0345, wR2 = 0.0890
Largest diff. peak and hole	1.455 and –0.788 e.A^{-3}

Table 8. Crystal data and structure refinement for lvp3n

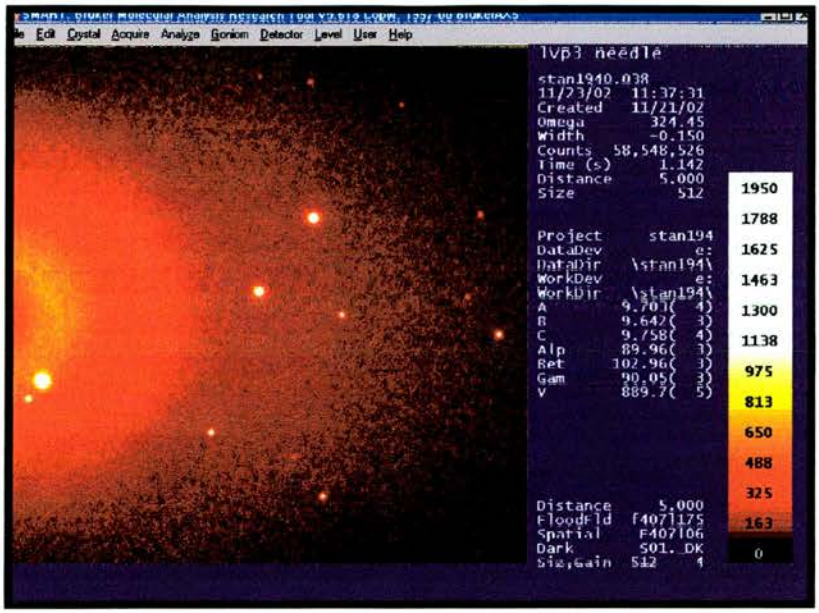

Figure 33. X-ray diffraction of the monoclinic crystal

Figure 33 shows a screenshot of a frame from a typical data collection using an area detector. Table 8 shows the crystal data obtained for the monoclinic crystal.

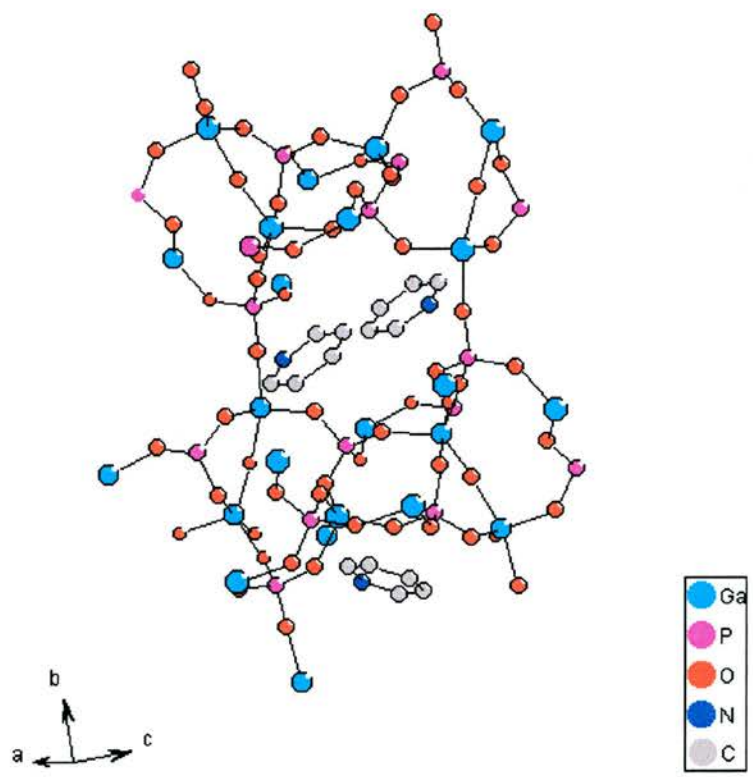

Figure 34. The crystal structure of lvp3n – the monoclinic phase

From figure 34, it can be clearly seen that the pyridine rings are situated inside the cages formed by the gallium, phosphate and oxygen linkages. The cages are eight ring windows which are visible along the a axis. In the diagram, gallium is blue, phosphorus is pink and the oxygens are red. It was discovered that the gallium did not only have one coordination site, but in fact two. Figure 35 will illustrate this more clearly.

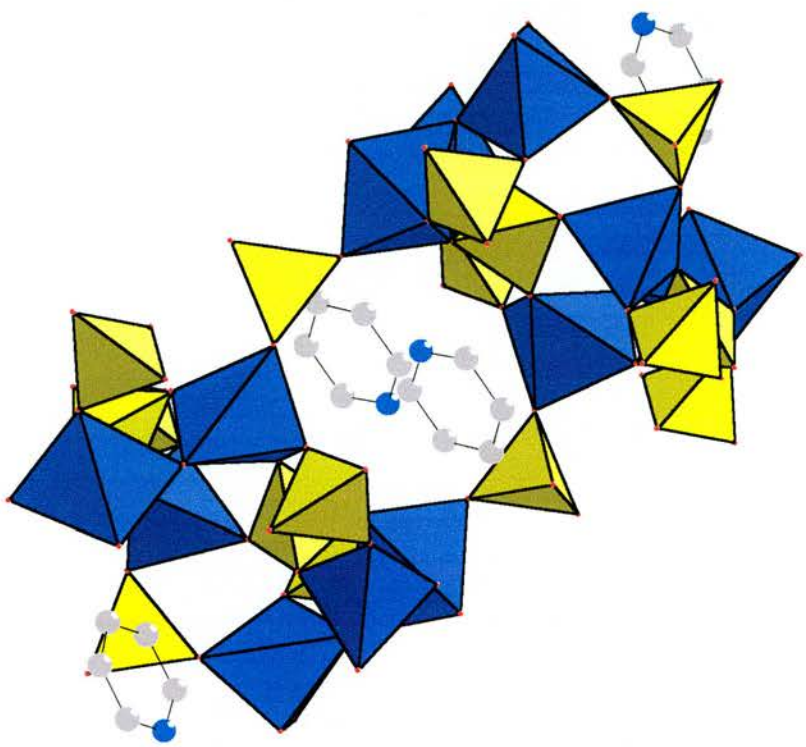

Figure 35. Coordination of Gallium (blue) and Phosphorus (yellow)

There are two different sites for gallium, which are indicated by the blue polyhedra in the picture. The gallium can either be trigonal bipyramidal or tetrahedral as shown. The phosphorus was discovered to be only tetrahedrally coordinated, and the yellow tetrahedral polyhedra illustrate this. Figure 36 shows the trigonal bipyramidal and tetrahedral co-ordination of the gallium bonds in the structure and how the oxygens link to the tetrahedral phosphorus.

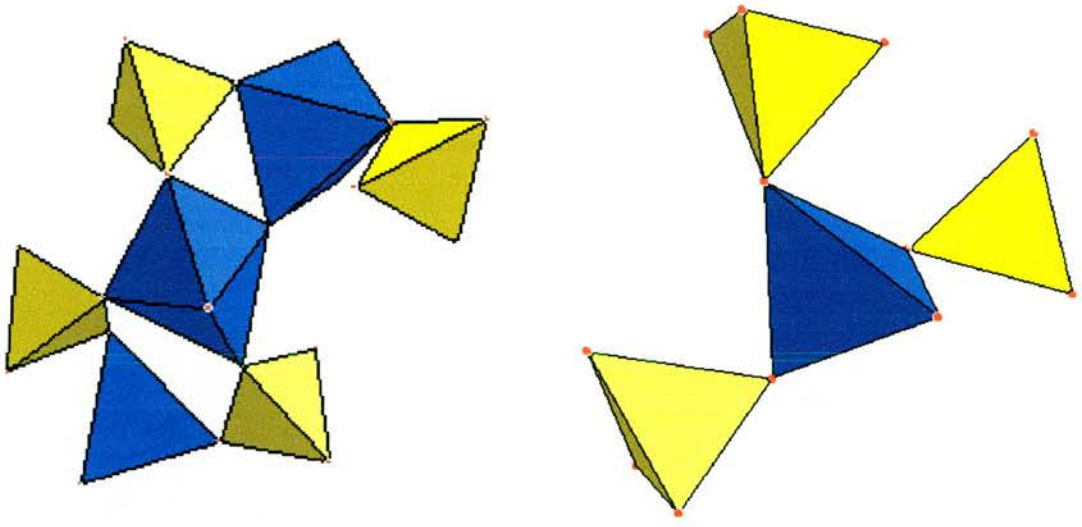

Figure 36 Co-ordination of the Gallium polyhedra in the Monoclinic crystal

In the picture on the left, the trigonal bipyramidal gallium, bonded to five oxygens, shares one of these with another one of its neighbouring bipyramidal polyhedra, linking the two together. The phosphorus polyhedra can be seen to bond to three sites on the gallium polyhedra, again linking through the oxygens. In the right picture, the blue tetragonal gallium bonds through three of its corner oxygens to three yellow phosphorus polyhedra. For bond lengths and angles see appendix section 7.1. Figure 37 shows 2 unit cells of the crystal structure.

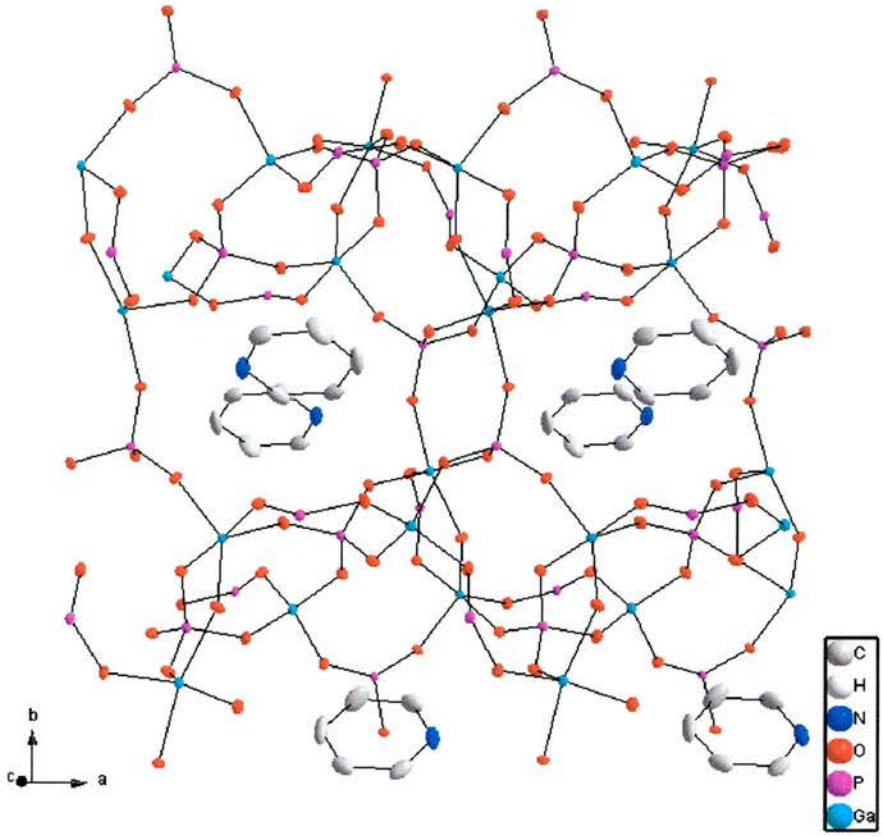

Figure 37. Lvp3n: A 2 unit cell thermal ellipsoid representation

Figure 37 shows the anisotropically refined atoms in the monoclinic crystal structure. It clearly shows how the unit cell repeats throughout the framework and the two pyridine molecules within the channels. Once refined anisotropically, the atoms appear as thermal ellipsoids. This takes into account the positions of the atoms within the crystal and the directions of vibrations.

This structure can be compared with other reported synthesised GaPO frameworks. Generally fluorine is added to help stabilize the double 4-rings in the structure, particularly in the gallium oxyfluorophosphate series. An example of this is ULM-5[3], a 16-membered ring synthesised from 1,6-diaminohexane and HF. Even with the discovery of these large pore materials, it is still rare to find a 14-membered ring

structure within this particular group. One example is the 14-membered ring phosphate, $AlPO_4$-8, which can only be obtained by the dehydration of VPI-5 at high temperatures. However there is another structure, DIPYR-GaPO.[4] The reason why this crystal framework is particularly important is that pyridine was used in its synthesis, just like in the synthesis of the monoclinic crystal. $Ga_2(SO_4)_3$, H_3PO_4, deionized water, pyridine, HF-pyridine and benzylviologen dichloride are the starting chemicals. Its crystal system is triclinic and has a space group of P1 compared to the monoclinic system and P $2_1/n$ spacegroup of the lvp3n crystal structure. The unit cell is 12 Å x 13 Å x 10 Å, with α, β, and $\gamma = 101.09^0$, 100.91^0 and 106.41^0 respectively. The framework consists of 4,5 and 6 coordinated gallium compared to the coordination of 4 and 5 in the lvp3n crystal. 2 pyridine molecules were located within the 8-ring membered pores of the lvp3n framework, however within the DIPYR-GaPO framework, there are 2 templates present: 4,4'-dipyridyl and pyridine. The benzylviologen dichloride decomposed during the reaction to form 4,4'-dipyridyl.

The diameter of the lvp3n pore 8-membered ring is approximately 8 Å, compared to the 14 ring channels of DIPY-GaPO. However the oxygens bridge similarly to that of DIPY-GaPO, between the galliums. In the DIPY-GaPO, the framework consists of 4, 5 and 6 coordinated gallium, however in the lvp3n crystal structure it has only the 4 and 5 coordination. The bond distances show the wide variation within the tetrahedral and trigonal bipyramidal framework too, equatorial oxygens range from 1.813 Å to 1.854 Å while the axial ones range from 1.818 Å to 1.962 Å. These results are very similar to the DIPY-GaPO, where the axial distances of the oxygens range from 1.856 Å to 1.962 Å. All of the linkages are through oxygens which bridge the galliums to the tetrahedral phosphorus.

5.2.4 Conclusion

This crystal data was refined to 3%, indicating that the model, which has been projected for this crystal, is extremely accurate. So it can be concluded that no double-four rings are still intact in this crystal structure. Most likely, the cubes broke up under the high temperature and underwent rearrangement to produce the small tetrahedral and trigonal bipyramidal units. It seems that this process was favoured over condensation of the actual D4R units. Eight ring atom windows can be clearly seen in the solid. The cages formed form these rings contain the pyridine molecules within them. Oxygen atoms in the rings are situated approximately 7.257(5) Å in opposition to one another, the gallium atoms 8.960(4) Å and the phosphorus atoms are 7.978(4) Å. So the diameter of the cages are between approximately 7-8 Å in length. It could be that the high temperatures are indicative of destroying the cube completely or too quickly; however this will need to be repeated with refined experimentation to ascertain whether this is true. So even though no double-four rings remained intact in the white crystalline solid produced, it does present an interesting question; at what point does the D4R actually decompose and how rapid is the outcome? Although no structure directing agents had been added to the original homogenised solution to help with linking the cubes, a crystalline solid was produced from a very simple hydrothermal synthesis.

5.2.5 Rhomboidal prism crystal

These crystals were analysed in exactly the same way as the monoclinic crystals from the lvp3 sample. The crystals were again too small for standard laboratory single-crystal X-ray diffractometers so diffraction data was collected on a Bruker AXS SMART CCD area-detector diffractometer on the high-flux single-crystal diffraction station 9.8 at CCLRC Daresbury Laboratory Synchrotron Radiation Source, Cheshire,

UK. Data reduction and cell refinements were carried out using Bruker SAINT packages. Structures were solved by direct methods (SHELXS-97) and refined with full-matrix least squares technique (SHELXL-97) using WinGX. All non-hydrogen atoms were refined anisotropically and hydrogen atoms were geometrically placed. Details of the data collected and the structure parameters are given in the tables for each structure.

5.2.6 Analysis of the Rhomboidal prism crystal

For the synthesis of this crystal see section 5.2.3.

Identification code	**Stan198/lvp3p**
Empirical formula	$H_{32}\ Ga_8\ O_{48}\ P_8$
Formula weight	1605.78
Temperature	293(2) K
Wavelength	0.69320 Å
Crystal system, space group	Monoclinic, P 1 2_1/n 1
Unit cell dimensions	a =9.6677(4) Å $\alpha = 90^0$
	b =9.6116(4) Å $\beta = 102.9610(10)^0$
	c =9.7461(4) Å $\gamma = 90^0$
Volume	882.55(6) A^3
Z, Calculated density	1, 3.021 Kg/m^3
Absorption coefficient	5.917 mm^{-1}
F(000)	784
Crystal size	0.06 x 0.06 x 0.02 mm
Theta range for data collection	2.62 to 29.40^0
Limiting indices	-13<=h<=7, -8<=k<=12, -12<=l<=13
Reflections collected / unique	3778 / 2116 [R(int) = 0.0343]
Completeness to theta = 29.40	80.6 %
Absorption correction	None
Refinement method	Full-matrix least-squares on F^2
Data / restraints / parameters	2116 / 0 / 145
Goodness-of-fit on F^2	1.091
Final R indices [I>2sigma(I)]	R1 = 0.0521, wR2 = 0.1505
R indices (all data)	R1 = 0.0529, wR2 = 0.1517
Largest diff. Peak and hole	1.825 and –1.682 $e.A^{-3}$

Table 9. Crystal data and structure refinement for stan198/lvp3p.

The diffraction process was repeated for this crystal, mounting it on a two-stage fibre and placing it in the diffractometer. Scattering from the beam is detected by an area detector.

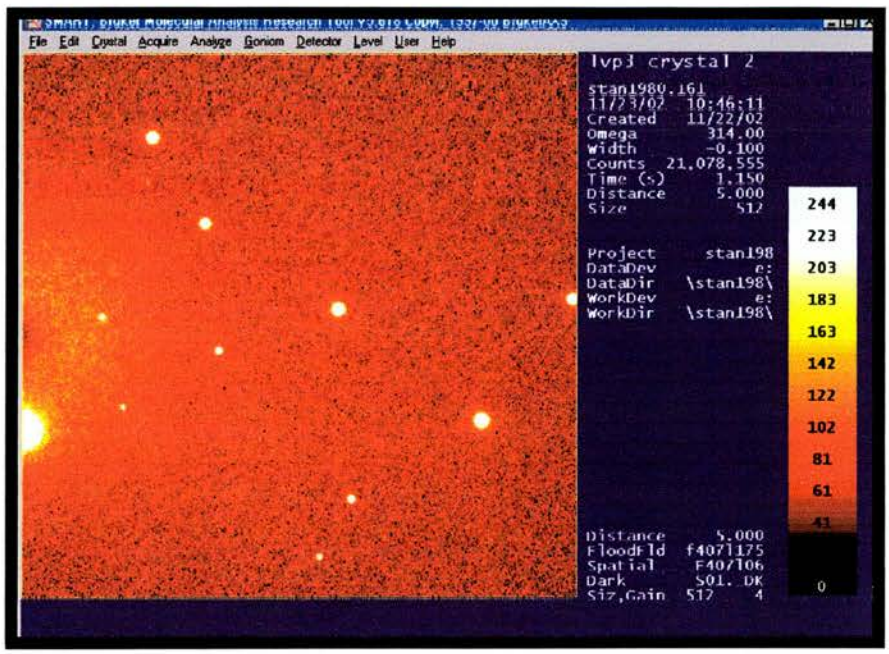

Figure 38. X-ray diffraction of the rhomboidal crystal

Figure 38 shows the screenshot of a frame from the data collection using an area detector. The a, b and c distances in the unit cell are approximately 9 Å each, making it smaller in comparison to the monoclinic unit cell. Refinement of the data has produced this detailed model of the crystal structure.

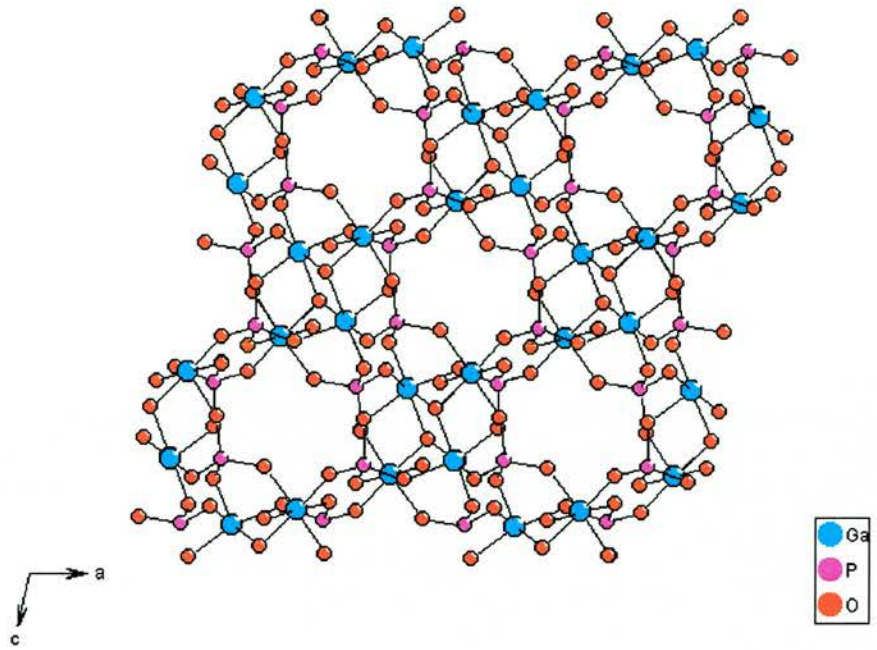

Figure 39. Rhomboidal prism crystal

The gallium was found in only one coordination site in this crystal, as opposed to the trigonal bipyramidal and tetrahedral sites in the first one. The position of the gallium indicates that it is octahedrally coordinated with the oxygens. The phosphorus is again tetrahedrally coordinated. Figure 40 shows more clearly the binding of the gallium and phosphorus to the oxygens, and shows the extent of the channel formation in the supercell. This is viewed down the b axis.

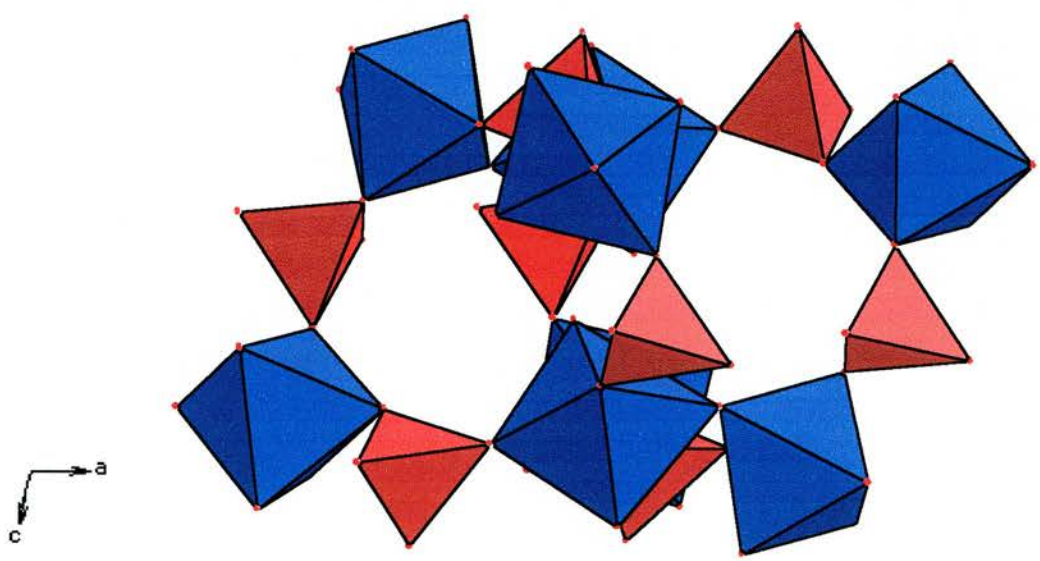

Figure 40. Coordination of gallium and phosphorus

In figure 40, gallium is represented by the blue octahedrons and phosphorus by the red tetrahedral structures. This unit cell is smaller than the monoclinic unit cell.

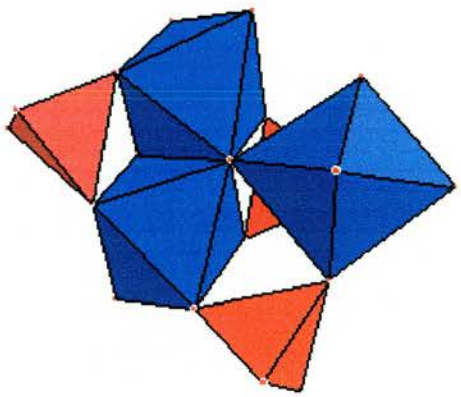

Figure 41. O_h Ga linking

An oxygen is bonded to and shared by three gallium atoms in figure 41. This diagram is taken from the refined supercell of the rhomboidal prism crystal. The red polyhedra again represent the tetrahedrally coordinated phosphorus atoms, which bond through two oxygens, each to different gallium atoms. The bond lengths and refinements are given in the appendix section 7.2.

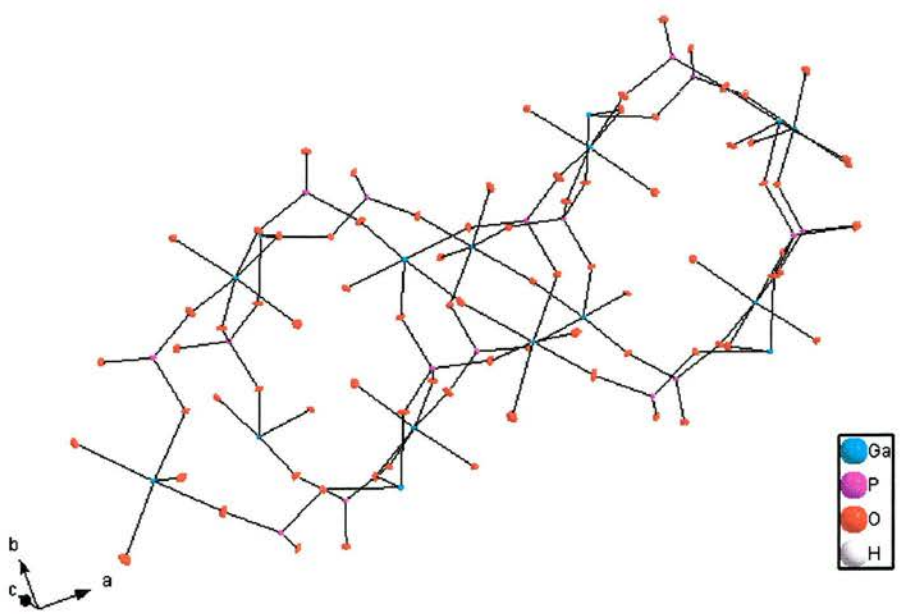

Figure 42. Lvp3p: A 2 unit cell thermal ellipsoid representation

The anisotropic refinement in figure 42 shows axial oxygens situated within the pores. Since the hydrogens are not shown for clarity, it is entirely possible that these oxygens are in fact hydroxyls. The distances between the blue gallium atoms and the axial oxygens are 2.017 Å in the octahedral, and the equatorial oxygen distances are approximately 1.931 Å. Unlike the previous crystal sample, with pyridine in lvp3n, no template was found within the channels. It is probable that water molecules are also located within the pores of the crystal framework. Comparing this structure with the previously mentioned DIPY-$GaPO^4$ crystal, it also has water molecules present within the framework. The water molecules form part of the coordination spheres of the octahedral galliums, and this could be happening here too. This was discovered during anisotropic refinement, however were left out for clarity in the diagram. This suggests that internal hydrogen bonding within the framework could help to govern the size of the pore. The oxygen-phosphorus distances within the phosphorus tetrahedral range between 1.5534 Å and 1.550 Å.

5.2.7 Conclusion

The crystal data was refined to 5% by the computer programme so the models shown are accurate. However, even though no hydrogens have been added into any diagrams, they were taken into account in the final formula. It is impossible to say for sure where exactly they are all are positioned in the crystal structure. During analysis it was discovered that as well as the hydrogens existing in hydroxyl groups within the structure, water molecules were also present. So, after detailed analysis it can be concluded that no double-four rings were present in the rhomboidal prism crystal structure. This result was to be expected as, like the monoclinic crystal, it was shown that the double-four ring units break up and disintegrate at temperatures that are too high for them to remain intact. To start off, the gallium cubes were actually synthesised

as the autoclave was put under a temperature of 150 ^{0}C for two days, but no cooling was allowed. The autoclave was removed from the oven and placed directly under a temperature of 190 ^{0}C. Perhaps if the sample had been cooled, washed and dried, this might have made a difference in the resulting solid. However, even though 190 ^{0}C is usually too high to produce any significant results it was interesting in this case, especially as this result was significantly better, in terms of crystalline structure, than the 170 ^{0}C sample. The fact that such diverse crystal types were produced from this particular crystalline material suggests that even though the temperature difference was only 20 ^{0}C between samples, huge structural diversities occurred. This proves just how unstable and inexact this type of hydrothermal synthesis actually is. It is extremely difficult to know which temperatures and which compositions will yield positive results and excellent examples of crystalline products.

5.3 A new approach to linking – Metal Ions

From the first part of this research, it is clear that something is required to link the cubes together, in an attempt to prevent the cubes from breaking up and disintegrating. The first idea is to add metal ions to the cubes in solution. The metal ions chosen to try and link the cubes together include barium, copper, zinc, calcium and silver. These 2+ ions will readily bond to oxygen, which is the bridging ion. Each oxygen itself is bonded to the eight corners of the cube, and with the introduction of the metal ion, should bond to the ion forming an ordered structure. Reactions carried out at room temperature include:

- $Ba(NO_3)_2 + H_2O$ + TMA silica cube
- $AgNO_3 + H_2O$ + TMA silica cube
- $Ca(NO_3)_2 + H_2O$ + TMA silica cube
- $Zn(CH_3CO_2)_2 + H_2O$ + TMA silica cube

These are just a few of the reactions using metal 2+ ions. They were left at room temperature over a period of two weeks. However, after the two weeks no crystalline products had formed. In some of the reaction vessels gels had precipitated out. Therefore the products were rapidly precipitating out, not allowing crystalline materials to form. Hence, no x-ray powder patterns could be collected. These mixtures were all filtered and washed. The filtrates from each were retained and allowed to evaporate off at room temperature; however, only solid masses remained once all of the solvent had evaporated off.

Other reactions involving methanol as the solvent this time were also carried out at room temperature. Although as before, fluffy-like gels precipitated out of the solution, unable to form any kind of crystalline material. The problem again was that the reactions were going too fast and not allowing any kind of cohesion between the silicate cubes and the metal ion compounds. So it was decided that for any kind of crystalline solid to be given a chance to form the temperature would have to be increased. None of the experiments at room temperature had worked so these particular reactions would now be carried out at much higher temperatures under hydrothermal synthesis. The exact same starting materials and solvents would be used under strictly controlled conditions.

Once set up inside the autoclaves, the reaction mixture was placed under temperatures ranging from 130 – 190 ^{0}C and left for a controlled period of time. Even after washing and drying no significant results were recovered from the autoclaves. The end products were all dark brown or black powders, unsuitable for further analysis. Even when the times of each synthesis were altered, this did not seem to make any difference to the end product. So the overall fact is that no successful crystalline solid was achieved from any synthesis in these sets of experiments. In no way involving 2+ metal ions, could the reaction be slowed down significantly enough for the cubes to react with the metal ion compounds in solution. Another way will have to be looked at to try to get the cubes to link together.

5.4 Mercury incorporated crystals

One of the main aims of this project was to incorporate mercury ions into the 'cubes', to try to get the building units to link linearly through the starting materials. Mercury has one important asset in that it favours bonding linearly. Results were produced from experiments that incorporated mercury chloride with the tetramethylammonium silicon based cube and methanol. In this particular sample $HgCl_2$, the TMA silica cube and CH_3OH were put under hydrothermal synthesis at 150 ^{0}C for three days.

Powder patterns were collected on a STOE STADIP diffractometer, see appendix section 7, figure 51. Initial results indicated that the synthesis of a new material had occurred due to a shift in the positions of the peaks, by comparison of figures 51 and 52 in the appendix section. Figure 52 shows the powder pattern for $HgCl_2$. It was discovered that two distinct crystal structure types were formed from this synthesis: the

needles (lprm3n) and the platelets (lprm3p). The structures were solved using a standard laboratory single-crystal x-ray diffractometer. Structures were solved by direct methods (SHELXS-97) and refined with the full-matrix least squares technique (SHELXL-97) using WinGX. All non-hydrogen atoms were refined anisotropically and hydrogen atoms were geometrically placed. Details of the data collected and the structure parameters are given in the tables for each structure.

5.4.1 Needle crystal

Identification code	**Lprm3n**
Empirical formula	C_{16} H_{64} Cl_{12} Hg_4 N_4
Formula weight	1540.47
Temperature	293(2)K
Wavelength	0.71073 Å
Crystal system, space group	Monoclinic, $P2_1$
Unit cell dimensions	a =7.549(2) Å $\alpha = 90^0$ b =15.689(5) Å $\beta = 93.621(9)^0$ c =8.862(2) Å $\gamma = 90^0$
Volume	1047.5(5) $Å^3$
Z, Calculated density	1, 2.442 Kg/m^3
Absorption coefficient	15.393 mm^{-1}
F(000)	712
Theta range for data collection	2.60 to 24.70^0
Limiting indices	-8<=h<=8, -18<=k<=12, -9<=l<=10
Reflections collected / unique	4058 / 2349 [R(int) = 0.0293]
Completeness to theta = 24.70	90.5%
Absorption correction	None
Refinement method	Full-matrix least-squares on F^2
Data / restraints / parameters	2349 / 1 / 163
Goodness-of-fit on F^2	0.668
Final R indices [I>2sigma(I)]	R1 = 0.0387, wR2 = 0.0987
R indices (all data)	R1 = 0.0443, wR2 = 0.1031
Absolute structure parameter	0.012(19)
Largest diff. Peak and hole	0.852 and -1.268 $e.Å^{-3}$

Table 10. Crystal data and structure refinement for lprm3n.

The unit cell is quite large, approximately the same size as the monoclinic crystal formed by the gallium cube. The first diagram for the needle crystal is shown in figure 43.

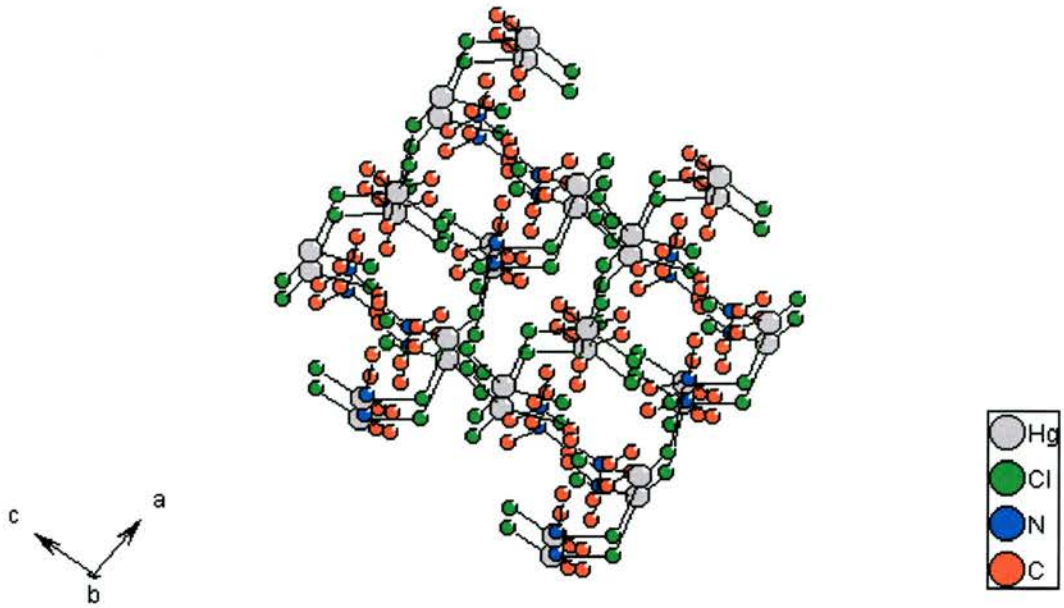

Figure 43. Mercury needle crystal

The diagram shows mercury bonded to four chlorines, with the mercury (grey), tetrahedrally co-ordinated. For clarity these are the only four elements present in the picture. This diagram illustrates very well the channels and possible cages running through the mercury incorporated crystals. Figure 44 illustrates more clearly the bonding between the atoms.

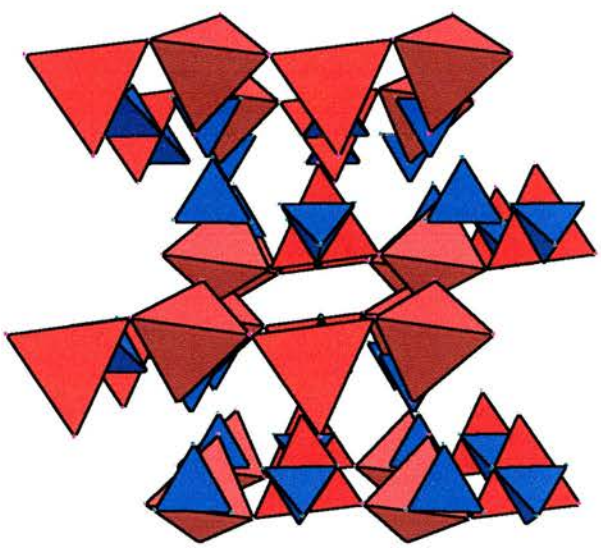

Figure 44. Co-ordination in the mercury crystal

The blue tetrahedral structures are the nitrogens bonded to carbons, while the reds are the mercury atoms tetrahedrally bonded to the chlorines. One tetrahedral mercury shares one of its corner chlorines with another tetrahedral mercury. Each one is rotated approximately 180^0 in relation to its neighbour. By linking through chlorines they form long chains in the overall crystalline structure. This can be seen from figure 45.

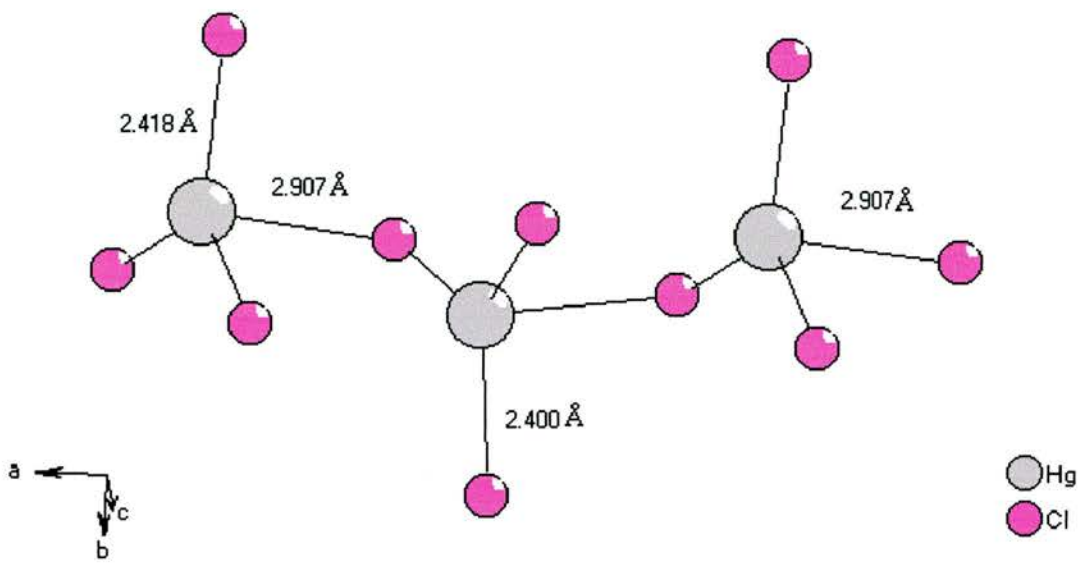

Figure 45. Mercury linking through the needle crystal.

The distance between the mercury and the bridging chlorine is 2.907 Å and is repeated one unit along. The other Hg-Cl distances go from 2.400 Å up to 2.418 Å. In the tetrahedra itself, the angles between the atoms range from 120.74^0 to 122.80^0, and 90.68^0 to 92.37^0. For the bridging chlorines, the angles are slightly different at 95.23^0 and 96.91^0.

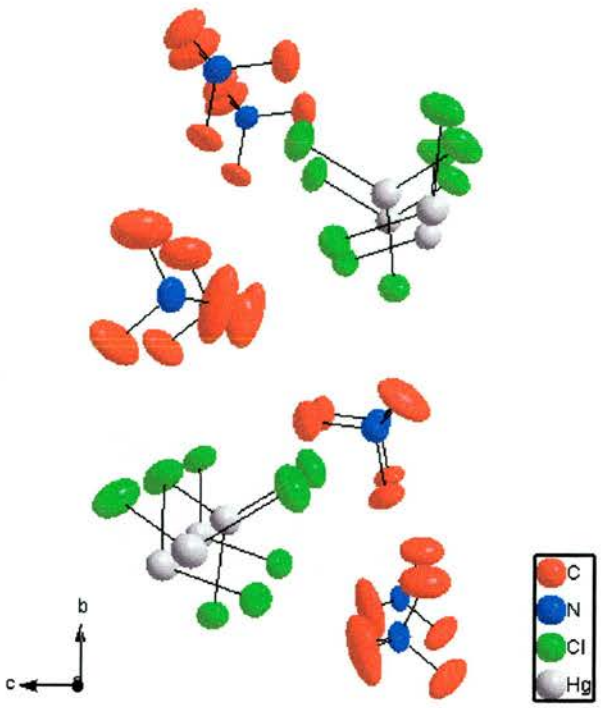

Figure 46. Lvp3n: A 2 unit cell anisotropically refined representation

Mercury (II) is a 'soft' cation, showing a preference for anions such as Cl, Br, I and S. It can have coordination numbers of 2 up to 6, however it does prefer the lower values. The reason why it was chosen for these experiments is that has a preference for the linear 2-coordination. In aqueous solutions mercury can form complexes with the formula HgX_n^{-n+2}. In other solvents such as methanol, the HgX_3^- species are favoured, which may have trigonal bipyramidal [$HgX_3S_2]^-$ or tetrahedral $[HgX_3S]^-$ structures (S = solvent).[6] Methanol was the solvent used in this particular experiment and it seems as if the mercury has formed a $HgCl_3^-$ complex, an intermediate in between a trigonal bipyramid and a tetrahedral. It is the equatorial chlorines that are the bridging atoms and seem to be almost planar with the mercury. The distance between the mercury and the equatorial chlorine is large, 2.907Å.

5.4.2 Conclusion

These crystals were very large and excellent to look at under the microscope, especially the long needle-like ones. The temperature chosen for synthesis was 150 ^{0}C, as any higher would probably result in complete disintegration of the TMA silica cubes. Within the structure, long chains of mercury chloride tetrahedra make up the layers along with the nitrogen tetrahedra. The overall structure and the linking throughout this crystal is different to what was predicted in the aims section. It was hoped that the mercury would bond to the silica based cube, via the O^- ions, each situated at the eight corners of the starting material. Hence, with the Hg^{2+} ion bonding twice to two different O^- ions, it would form a linear bond with two cubes and therefore a very ordered crystalline structure. As this did not happen, possibly the TMA silica based cubes did indeed break up and remain in solution, unable to isomerise.

5.4.3 Platelet crystal

These crystals are a lot smaller the needle-like counterparts found in the same sample. The cell density is approximately 1/5 compared to the needle crystals. A powder pattern was collected on a STOE STADIP diffractometer, see figure 51 in the bibliography section. The structures were then solved using a standard laboratory single-crystal x-ray diffractometer. Structures were solved by direct methods (SHELXS-97) and refined with full-matrix least squares technique (SHELXL-97) using WinGX. All non-hydrogen atoms were refined anisotropically. Details of the data collected and the structure parameters are given in the tables for each structure.

Identification code	Lprm3p
Empirical formula	$Cl_4 Hg_4$
Formula weight	944.16
Temperature	293(2) K
Wavelength	0.71073 Å
Crystal system, space group	Monoclinic, C 1 2 1
Unit cell dimensions	a =11.771(2) Å $\alpha = 90^0$
	b =4.4832(9) Å $\beta = 112.28(3)^0$
	c =4.4822(9) Å $\gamma = 90^0$
Volume	218.87(8) $Å^3$
Z, Calculated density	1, 7.163 Kg/m^3
Absorption coefficient	71.051 mm^{-1}
F(000)	388
Theta range for data collection	3.74 to 24.32^0
Limiting indices	-10<=h<=13, -3<=k<=5, -5<=l<=4
Reflections collected / unique	355 / 244 [R(int) = 0.0795]
Completeness to theta = 24.32	82.9%
Absorption correction	None
Refinement method	Full-matrix least-squares on F^2
Data / restraints / parameters	244 / 7 / 19
Goodness-of-fit on F^2	1.923
Final R indices [I>2sigma(I)]	R1 = 0.1172, wR2 = 0.2710
R indices (all data)	R1 = 0.1184, wR2 = 0.2726
Absolute structure parameter	-0.1(2)
Largest diff. Peak and hole	4.920 and –5.163 $e.A^{-3}$

Table 11. Crystal data and structure refinement for lprm3p.

The unit cell for this crystal is small, a = 11.771 Å x b = 4.4832 Å x c = 4.4822 Å, compared to the dimensions for lprm3n, the needle crystal. After detailed analysis it was discovered that this new structure did not integrate any of the Si^{4+} atoms into the architecture. Figure 47 shows the structure of lprm3p, the platelet crystal.

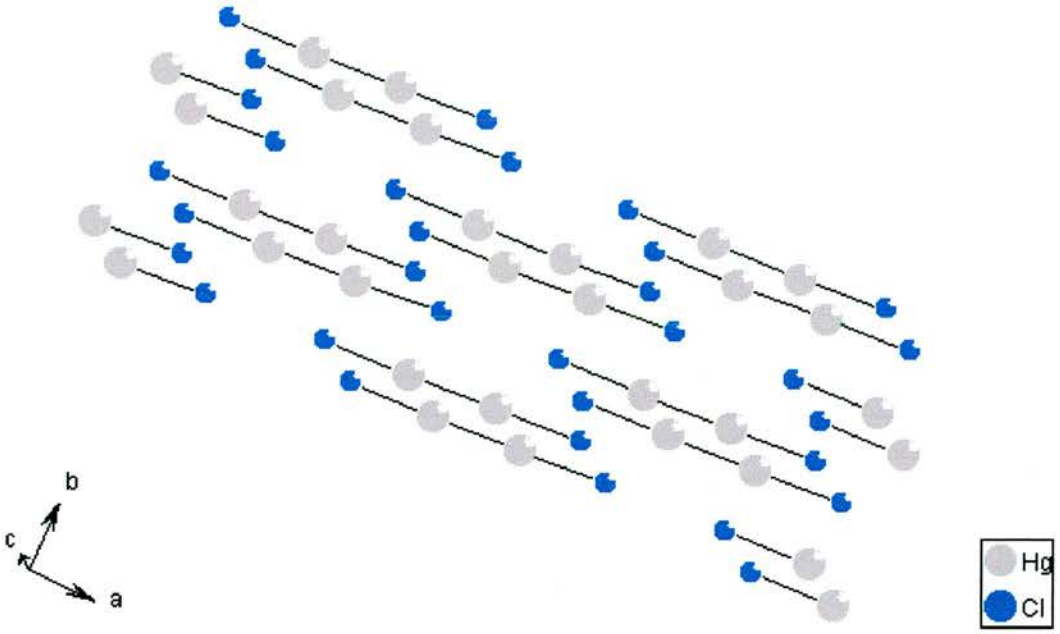

Figure 47. Mercury platelet crystal

As can be seen from the diagram, the mercury chloride crystals are planes of linear molecules. The distances between each mercury atom is 2.532(31) Å, between a mercury and chlorine molecule is 2.459(31) Å, and finally between the planes themselves the distance is approximately 3.259(9) Å. The formula is Hg_2Cl_2. This is a new form (polymorph) of Hg_2Cl_2, the previously known version being tetragonal, although the unit cell is closely related to one synthesised in 1989.[1] That unit cell was approximately 10 Å x 4 Å x 4 Å, with α,β and $\gamma = 90^0$. This crystal, lprm3p, has a unit cell of 11.771 Å x 4.483 Å x 4.482 Å, but $\beta = 112.28^0$.

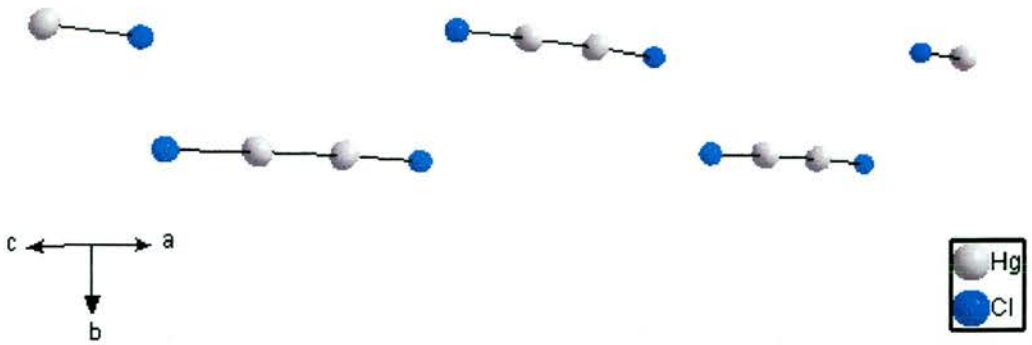

Figure 48. Lprm3p: A 2 unit cell anisotropically refined representation

5.4.4 Conclusion

The first of these crystals was monoclinic with spacegroup $P2_1/n$, primitive, and had a fairly large unit cell with the dimensions 7.548 Å by 15.688 Å by 8.862 Å. The platelets are also monoclinic with the spacegroup C 2_1, face-centered, and the unit cell has dimensions 11.771 Å by 4.483 Å by 4.482 Å. These figures illustrate the difference between the two crystals, the needles and the platelets. The mercury in this mercury chloride crystal structure has been converted into Hg_2^{2+}, while no Si^{4+} atoms had been incorporated into the overall structure. Between both results from this particular sample, it appears that the mercury favours bonding to the chlorine ion, rather than the silicon. Both results incorporate the mercury, but not in the way that was hoped, with the mercury bonding through oxygens on the corners of the tetramethylammonium silica cube.

5.5 Organic group: Dipyridine dihydrochloride

No notable results were produced from any of the previous sections regarding experimentation with the cubes and trying to get them to link together with metal ions

such as barium, silver, copper, zinc or even mercury compounds. Therefore the next stage was to introduce organic linkers as opposed to the metal ions. The linkers chosen were imidazole hydrochloride and dipyridinium dihydrochloride. These organic compounds could introduce rigidity to the overall structure and make it more stable. Crystals were formed from the filtrate of the dipyridine dihydrochloride sample with methanol. The solvent was allowed to evaporate from the filtrate at room temperature for a period of two weeks. During this time needle-like crystals were produced.

5.5.1 Single-crystal X-ray diffraction

A powder pattern was collected on a STOE STADIP diffractometer. The structure was then analysed using a standard laboratory single-crystal x-ray diffractometer, solved by direct methods (SHELXS-97) and refined with full-matrix least squares technique (SHELXL-97) using WinGX. Details of the data collected and the structure parameters are given in the table. The sample analysed on the in-house single crystal x-ray diffractor was:

- Dipy with the TMA - Silicon based cube in methanol

Structures identified by the single-crystal diffractor include previously synthesised dipyridine dihydrochloride crystals. The product was a white crystalline solid.

5.5.2 Dipyridine dihydrochloride crystal in CH_3OH

Identification code	Lprm4
Empirical formula	$C_{40}\ H_{52}\ Cl_4\ N_8\ O_8$
Formula weight	914.70
Temperature	125(2) K
Wavelength	0.71073 Å
Crystal system, space group	Orthorhombic, P n m a
Unit cell dimensions	a= 9.778(3) Å $\alpha= 90^0$ b= 7.108(3) Å $\beta= 90^0$ c= 15.718(5) Å $\gamma= 90^0$
Volume	1092.3(7) $Å^3$
Z, Calculated density	1, 1.390 Kg/m^3
Absorption coefficient	0.332 mm^{-1}
F(000)	480
Theta range for data collection	2.45 to 23.26^0
Limiting indices	-10<=h<=10, -7<=k<=7, -17<=l<=15
Reflections collected / Unique	4496 / 855 [R(int) = 0.0746]
Completeness to theta = 23.26	99.9%
Absorption correction	None
Refinement method	Full-matrix least-squares on F^2
Data / restraints / Parameters	855 / 12 / 88
Goodness-of-fit on F^2	0.957
Final R indices [I>2sigma(I)]	R1 = 0.0661, wR2 = 0.2228
R indices (all data)	1 = 0.0958, wR2 = 0.2586
Largest diff. Peak and hole	0.589 and –0.435 $e.A^{-3}$

Table 12. Crystal data and structure refinement for lprm4.

The dipyridine dihydrochloride crystals had been previously synthesised, although this is a new method. The chlorine is now situated in between the planes of the assembled rings. For every molecule of dipyridine, there is one chlorine molecule. Analysis shows that there are probably water molecules sitting in the voids between the rows of dipyridine molecules, with the chlorine ions charge balanced. It is impossible to tell which of the nitrogens are protonated. The distance between each chlorine is approximately 5 Å and the rings do not form chains.

5.5.3 Conclusion

This shows that from the filtrate no new products were present. It is only the excess dipyridenium crystals that form. Elements from the starting material, which was the tetramethylammonium silica based cube, were not present in these particular crystals. The solid that precipitated out after fourteen days was a white powder. After washing and drying, it was not possible to put it under single crystal X-ray diffraction. It was hoped that the crystals from the filtrate would contain some of the starting material, but they did not. The sample that contained isopropanol with the dipy and the $GaPO_4$ cube gave similar results, with the initial starting product dipyridenium dihydrochloride crystallising out. No cube was incorporated into any of these crystalline products.

5.6 Gallium Phosphate crystals

Excellent crystal specimens of the gallium cube were collected from two very different syntheses. Both of the autoclaves were placed in the same temperature of 150 ^{0}C, but were left under this temperature for very different lengths of time. Each contained the same chemicals necessary for the production of the gallium cube. The first sample produced excellent crystals, ones large enough to be analysed on the in-house x-ray diffractor. It had been under 150 ^{0}C for fourteen days. Unfortunately, it was not the gallium cube that was synthesised but gallium phosphate crystals.

5.6.1 Single-crystal X-ray diffraction

A powder pattern was collected on a STOE STADIP diffractometer, see appendix section 7.0 figure 53. The crystal samples were again analysed using the standard laboratory single-crystal x-ray diffractor. Structures were solved by direct methods

(SHELXS-97) and refined with full-matrix least squares technique (SHELXL-97) using WinGX. Details of the data collected and the structure parameters are given in the tables for each structure.

5.6.2 $GaPO_4$ cube data

Identification code	**Lprm6**
Empirical formula	Ga O_4 P
Formula weight	164.69
Temperature	293(2) K
Wavelength	0.71073 Å
Crystal system, space group	Orthorhombic, P n m a
Unit cell dimensions	a = 4.8992(7) Å alpha = 90^0
	b = 4.8992(7) Å beta = 90^0
	c = 11.043(2) Å gamma = 120^0
Volume	229.55(7) $Å^3$
Z, Calculated density	3, 3.574 Kg/m^3
Absorption coefficient	9.331 mm^{-1}
F(000)	234
Theta range for data collection	4.80 to 24.76^0
Limiting indices	-5<=h<=3, -4<=k<=5, -11<=l<=11
Reflections collected / unique	570 / 214 [R(int) = 0.0177]
Completeness to theta = 24.76	86.5%
Absorption correction	None
Refinement method	Full-matrix least-squares on F^2
Data / restraints / parameters	214 / 0 / 29
Goodness-of-fit on F^2	1.245
Final R indices [I>2sigma(I)]	R1 = 0.0297, wR2 = 0.0751
R indices (all data)	R1 = 0.0299, wR2 = 0.0754
Absolute structure parameter	0.19(7)
Largest diff. peak and hole	0.633 and –1.021 $e.A^{-3}$

Table 13. Crystal data and structure refinement for lprm6.

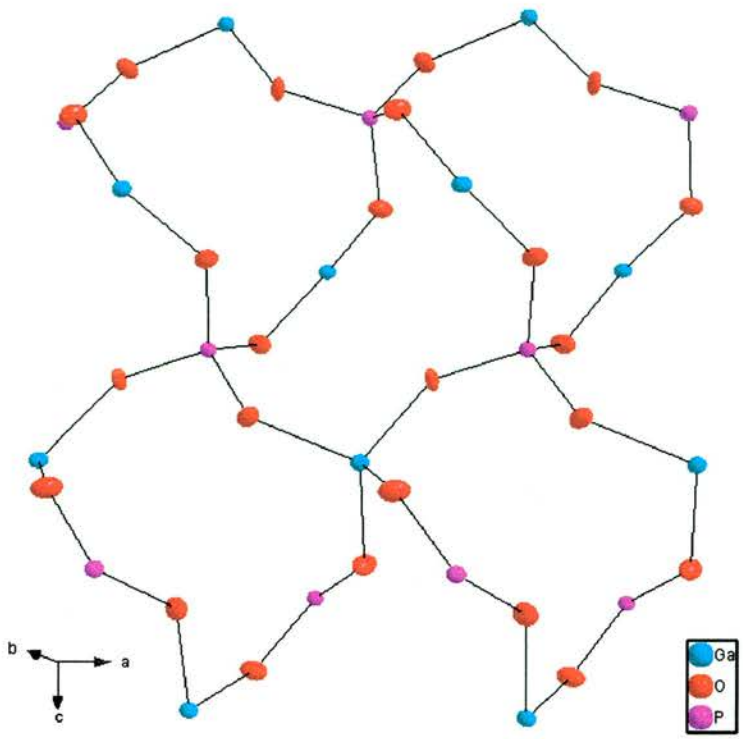

Figure 49. $GaPO_4$: A 2 unit cell anisotropically refined representation

5.6.3 Conclusion

The second sample, which was kept under 150 ^{0}C for a longer period of time, five months, did not produce crystals of the same size as the previous one. However, the crystals were still extremely crystalline and when analysed, showed that they had the same unit cell parameters as a previously known crystal structure, Berlinite[2]. Even under extreme conditions for long periods of time, it is difficult to say what will happen to the starting materials during this synthesis. It is not known at what point the cubes actually break up to undergo rearrangement or isomerisation.

5.7 $GaPO_4$ cubes incorporating Cyclam and Imidazole hydrochloride

No crystals were being produced from the autoclaves that contained the $GaPO_4$ cubes at temperatures of 150 ^{0}C and higher. However, results did come from the autoclaves that were under hydrothermal synthesis at 90 ^{0}C for fourteen days. Crystalline materials were formed from:

- $GaPO_4$ cube + Cyclam + $Cu(NO_3)_2.3H_2O$ + H_2O
- $GaPO_4$ cube + Imidazole hydrochloride + H_2O

These crystals could be the first ones produced from the incorporation of the $GaPO_4$ cube with cyclam, a copper (II) compound and imidazole hydrochloride. They were due to be taken down to the synchrotron radiation source at Daresbury on July 11th for analysis, but unfortunately this did not happen as the beam was down. These crystals have not fully been analysed by the in house diffractometers at St.Andrews.

5.8 The Germanate cube

The results show that crystals were only produced from reactions that incorporated the gallium phosphate and tetramethylammonium silica based analogues. As the crystals produced were of a good size and easily analysed, more reactions were carried out which included these starting materials. Attempts were also made at synthesising the germanate analogue. However, these attempts were unsuccessful in producing the complete cubic structure, so no further experiments were performed using this particular starting material.

5.9 References:

1) N. J. Carlos, C. H. L. Kennard. R. L. Davis, (1989), *Z. Kristallogr.*, **187**, 305-307

2) Kolodiev B. N., Lyutin V. I., Motchanyi A. I., Shvanskii P. P., *Inorg. Mat.,* 1999, **35**(70), 737-739

3) T. Loiseau, G. Férey, *J. Solid State Chem*, 1994, **111**, 403

4) Scott J. Weigel , Russell E. Morris , Galen D. Stucky and Anthony K. Cheetham, *J. Mater. Chem.*, 1998 **8** (7), 1607-1611

5) F. Cotton and G. Wilkinson, *Advanced Inorganic Chemistry*, Wiley-Interscience, UK, 1999, 6th Edition.

6.0 Further work

This research has shown that hydrothermal synthesis can be an extremely diverse and unpredictable process, with many factors influencing the outcome of the overall product. There is no exact method to produce microporous crystalline results. Many variables control the synthesised architecture of the solid, such as time, temperature, pH, structure-directing agent and the starting materials used. The aims section of this research described in detail what we hoped to achieved overall, however no such synthesis resulted in the production of these crystalline materials, in the way that was expected.

The effect of higher temperature does not affect the silica and gallium based cubes to the same extent. Results from the first set of experiments indicated that reactions involving the gallium cube at higher temperatures of 190 ^{0}C are not necessarily poor. Even though the cubes break up they do not disintegrate completely, but instead give crystalline solids with excellent architectures.

Lower temperatures seem to allow the starting materials in the solution to react together in a more feasible manner. Higher temperatures possibly force the cube to break up and disintegrate more quickly, not giving the D4Rs time to react as complete cubes with other chemical compounds such as cyclam or imidazole hydrochloride. So even though reactions at 90 ^{0}C were fairly successful, other temperatures could be tried out. For example, putting the autoclaves into an oven at 90 ^{0}C for seven days, removing them and placing them in an oven at 150 ^{0}C for a further seven days. Many autoclaves could be set up, with one as the standard that would be kept in the 90 ^{0}C oven and only removed at the end of the experiment. Two sets of experiments could be running simultaneously, autoclaves with the gallium cubes plus other structure-directing agents, and also a set

which included the silica based cube with the same chemical constituents. Most of the reactions were under the range of temperatures of 130 ^{0}C to 190 ^{0}C. Even though the majority of reactions were unsuccessful, it is still important that exhaustive research continues in this area.

It would be interesting to see if varying the concentrations were to make a significant difference in the overall structure. The ratios that were used in most of the reactions were 1: 4, so that no chemical was in excess of another. Changing the mole ratio to accommodate an excess of 2+ ions or organic/metal-organic linker compounds, could alter the reaction.

The implications of using alkali-earth metal ions as structure-directing agents with the 'cubes' could be investigated. Strontium and calcium could be introduced this time to study the effect of the 2+ ions at room temperature with the starting materials. The pH in many of the solutions before heating was very high so possibly the addition of an acidic-based compound could alter the outcome. More experiments should be carried out on the cubes with dipyridinium dihydrochloride, cyclam and imidazole hydrochloride. The recent results from cyclam in particular, suggest that exploring it as a metal-organic linker is essential.

Mixtures incorporating the gallium and silica based cubes with the organic and metal ion linkers could be placed for very long periods of time under many different temperatures. For most of the experiments in the research, the longest that an autoclave, other than containing the ordinary D4Rs, was under hydrothermal synthesis was three weeks. This time period could be extended to maybe eight weeks or possibly months at a time.

However, it would have to be under lower temperatures in order to avoid complete disintegration of the starting materials.

The tetramethylammonium silica based cube along with the gallium phosphate D4R unit both produced results worthy of analysis. However, difficulties were encountered with the germanate analogue. Once this D4R unit is properly synthesised, many of these reactions could be repeated using the germanate 'cube' as the starting material, including experiments with mercuric chloride and 1,4,8,11-tetraazocyclotetradecane.

7.0 Appendix

Supplementary information is supplied for some of the crystal structures; bond lengths, angles and anisotropic displacement parameters.

Figure 50 – lvp3

Figure 51 – lvp16on

Figure 52 – $HgCl_2$

Figure 53 – lvp51

7.1 Crystal Data: Stan 194/lvp3n

Ga(1)-O(4)	1.8537(19)
Ga(1)-O(6)	1.8858(18)
Ga(1)-O(5)	1.891(2)
Ga(1)-O(1)	1.9375(19)
Ga(1)-O(7)	1.962(2)
Ga(2)-O(12)#1	1.8701(18)
Ga(2)-O(8)	1.872(2)
Ga(2)-O(13)#1	1.8845(19)
Ga(2)-O(11)#2	1.9505(19)
Ga(2)-O(5)	1.9631(19)
Ga(3)-O(10)#3	1.8117(19)
Ga(3)-O(9)#1	1.8129(19)
Ga(3)-O(2)	1.8180(19)
Ga(3)-O(3)	1.819(2)
P(4)-O(6)#4	1.5188(19)
P(4)-O(12)	1.524(2)
P(4)-O(9)	1.536(2)
P(4)-O(3)	1.542(2)
P(5)-O(7)#5	1.517(2)
P(5)-O(1)	1.536(2)
P(5)-O(8)	1.537(2)
P(5)-O(10)	1.5453(18)
P(6)-O(13)	1.521(2)
P(6)-O(11)	1.522(2)
P(6)-O(4)	1.5242(19)
P(6)-O(2)	1.5404(18)
O(6)-P(4)#6	1.5188(19)
O(7)-P(5)#1	1.517(2)
O(9)-Ga(3)#5	1.8129(19)
O(10)-Ga(3)#7	1.8117(19)
O(11)-Ga(2)#8	1.9505(19)
O(12)-Ga(2)#5	1.8701(18)
O(13)-Ga(2)#5	1.8844(19)
N(1)-C(5)	1.317(4)
N(1)-C(6)	1.318(5)
C(2)-C(5)	1.353(5)
C(2)-C(3)	1.380(5)
C(3)-C(4)	1.385(5)
C(4)-C(6)	1.370(5)
O(4)-Ga(1)-O(6)	108.06(9)
O(4)-Ga(1)-O(5)	131.31(9)
O(6)-Ga(1)-O(5)	120.49(9)
O(4)-Ga(1)-O(1)	91.05(8)
O(6)-Ga(1)-O(1)	93.19(8)
O(5)-Ga(1)-O(1)	89.89(8)
O(4)-Ga(1)-O(7)	86.01(8)
O(6)-Ga(1)-O(7)	92.93(8)
O(5)-Ga(1)-O(7)	87.95(8)
O(1)-Ga(1)-O(7)	173.79(8)
O(12)#1-Ga(2)-O(8)	104.79(9)
O(12)#1-Ga(2)-O(13)#1	113.48(8)
O(8)-Ga(2)-O(13)#1	141.47(9)
O(12)#1-Ga(2)-O(11)#2	90.82(8)
O(8)-Ga(2)-O(11)#2	84.83(8)
O(13)#1-Ga(2)-O(11)#2	90.20(8)
O(12)#1-Ga(2)-O(5)	103.12(8)

O(8)-Ga(2)-O(5)	91.03(8)
O(13)#1-Ga(2)-O(5)	84.76(8)
O(11)#2-Ga(2)-O(5)	166.05(8)
O(10)#3-Ga(3)-O(9)#1	108.84(9)
O(10)#3-Ga(3)-O(2)	102.66(9)
O(9)#1-Ga(3)-O(2)	106.05(9)
O(10)#3-Ga(3)-O(3)	112.93(9)
O(9)#1-Ga(3)-O(3)	112.60(9)
O(2)-Ga(3)-O(3)	113.08(9)
O(6)#4-P(4)-O(12)	108.96(11)
O(6)#4-P(4)-O(9)	110.95(11)
O(12)-P(4)-O(9)	108.77(11)
O(6)#4-P(4)-O(3)	111.11(11)
O(12)-P(4)-O(3)	109.81(11)
O(9)-P(4)-O(3)	107.21(11)
O(7)#5-P(5)-O(1)	109.60(11)
O(7)#5-P(5)-O(8)	108.62(11)
O(1)-P(5)-O(8)	111.80(11)
O(7)#5-P(5)-O(10)	111.16(11)
O(1)-P(5)-O(10)	109.99(11)
O(8)-P(5)-O(10)	105.62(11)
O(13)-P(6)-O(11)	111.81(11)
O(13)-P(6)-O(4)	111.69(11)
O(11)-P(6)-O(4)	105.84(11)
O(13)-P(6)-O(2)	108.48(11)
O(11)-P(6)-O(2)	108.75(11)
O(4)-P(6)-O(2)	110.24(11)
P(5)-O(1)-Ga(1)	126.39(11)
P(6)-O(2)-Ga(3)	139.02(13)
P(4)-O(3)-Ga(3)	127.55(12)
P(6)-O(4)-Ga(1)	149.90(13)
Ga(1)-O(5)-Ga(2)	142.51(11)
P(4)#6-O(6)-Ga(1)	145.82(14)
P(5)#1-O(7)-Ga(1)	143.41(12)
P(5)-O(8)-Ga(2)	133.39(12)
P(4)-O(9)-Ga(3)#5	132.13(12)
P(5)-O(10)-Ga(3)#7	134.84(13)
P(6)-O(11)-Ga(2)#8	150.97(13)
P(4)-O(12)-Ga(2)#5	134.36(12)
P(6)-O(13)-Ga(2)#5	132.78(12)
C(5)-N(1)-C(6)	122.8(3)
C(5)-C(2)-C(3)	118.8(3)
C(2)-C(3)-C(4)	118.9(3)
C(6)-C(4)-C(3)	119.4(3)
N(1)-C(5)-C(2)	120.8(3)
N(1)-C(6)-C(4)	119.2(3)

Table 1. Bond lengths [Å] and angles [^{0}] for stan194.
Symmetry transformations used to generate equivalent atoms:
#1 x+1/2,-y+1/2,z+1/2 #2 -x+3/2,y+1/2,-z+1/2
#3 x-1/2,-y+1/2,z+1/2 #4 x-1,y,z
#5 x-1/2,-y+1/2,z-1/2 #6 x+1,y,z
#7 x+1/2,-y+1/2,z-1/2 #8 -x+3/2,y-1/2,-z+1/2

	U11	U22	U33	U23	U13	U12
Ga(1)	8(1)	7(1)	8(1)	0(1)	6(1)	0(1)
Ga(2)	9(1)	7(1)	7(1)	0(1)	5(1)	0(1)
Ga(3)	9(1)	10(1)	8(1)	-1(1)	6(1)	0(1)
P(4)	9(1)	9(1)	8(1)	1(1)	6(1)	1(1)
P(5)	9(1)	7(1)	7(1)	0(1)	5(1)	0(1)
P(6)	8(1)	6(1)	8(1)	0(1)	5(1)	0(1)
O(1)	11(1)	9(1)	10(1)	0(1)	4(1)	0(1)
O(2)	12(1)	11(1)	14(1)	-2(1)	10(1)	1(1)
O(3)	13(1)	10(1)	14(1)	-1(1)	3(1)	2(1)
O(4)	10(1)	9(1)	13(1)	2(1)	4(1)	-2(1)
O(5)	13(1)	10(1)	13(1)	-3(1)	4(1)	2(1)
O(6)	14(1)	13(1)	11(1)	0(1)	10(1)	2(1)
O(7)	12(1)	9(1)	13(1)	0(1)	4(1)	0(1)
O(8)	14(1)	11(1)	10(1)	-1(1)	5(1)	3(1)
O(9)	12(1)	13(1)	13(1)	4(1)	8(1)	3(1)
O(10)	12(1)	14(1)	13(1)	-2(1)	10(1)	-2(1)
O(11)	11(1)	6(1)	15(1)	2(1)	6(1)	0(1)
O(12)	11(1)	11(1)	11(1)	0(1)	8(1)	2(1)
O(13)	10(1)	13(1)	11(1)	1(1)	6(1)	1(1)
N(1)	15(1)	29(2)	30(2)	-10(1)	12(1)	-4(1)
C(2)	38(2)	18(2)	26(2)	-2(1)	22(2)	-6(1)
C(3)	15(1)	48(2)	29(2)	-13(2)	12(1)	0(1)
C(4)	40(2)	48(2)	21(2)	13(2)	9(2)	22(2)
C(5)	31(2)	24(2)	16(2)	1(1)	6(1)	12(1)
C(6)	41(2)	24(2)	30(2)	4(1)	24(2)	-3(2)

Table 2. Anisotropic displacement parameters (A^2 x 10^3) for stan194. The anisotropic displacement factor exponent takes the form: $-2\pi^2 [h^2 a^{*2} U11 + ... + 2 h k a^* b^* U12]$

	x	y	z	U(eq)
Ga(1)	9195(1)	2025(1)	1977(1)	7(1)
Ga(2)	8694(1)	3894(1)	3346(1)	7(1)
Ga(3)	4533(1)	1848(1)	2853(1)	8(1)
P(4)	1700(1)	2019(1)	17(1)	8(1)
P(5)	7370(1)	3322(1)	-68(1)	7(1)
P(6)	6435(1)	761(1)	1367(1)	7(1)
O(1)	7438(2)	2507(1)	467(2)	10(1)
O(2)	5199(2)	1003(1)	2140(2)	11(1)
O(3)	3039(2)	2351(1)	1363(2)	13(1)
O(4)	7958(2)	1201(1)	2034(2)	11(1)
O(5)	9587(2)	2910(1)	3166(2)	12(1)
O(6)	10267(2)	1837(1)	521(2)	11(1)
O(7)	10833(2)	1540(1)	3657(2)	11(1)
O(8)	7475(2)	3869(1)	1262(2)	11(1)
O(9)	1289(2)	2598(1)	-1292(2)	12(1)
O(10)	8808(2)	3499(1)	-620(2)	12(1)

O(11)	6864(2)	-51(1)	1770(2)	10(1)
O(12)	2271(2)	1309(1)	-564(2)	10(1)
O(13)	5743(2)	876(1)	-369(2)	11(1)
N(1)	9881(3)	265(2)	7021(3)	23(1)
C(2)	7806(4)	-26(2)	7963(4)	25(1)
C(3)	6786(4)	356(2)	6743(4)	29(1)
C(4)	7387(5)	709(2)	5691(4)	36(1)
C(5)	9348(4)	-70(2)	8051(4)	24(1)
C(6)	8966(5)	655(2)	5861(4)	29(1)

Table 3. Atomic coordinates (x 10^4) and equivalent isotropic displacement parameters (A^2 x 10^3) for stan194.
U(eq) is defined as one third of the trace of the orthogonalized Uij tensor.

7.2 Crystal Data: Stan 198/lvp3p

Ga(1)-O(8)	1.900(3)
Ga(1)-O(10)	1.903(3)
Ga(1)-O(6)	1.931(3)
Ga(1)-O(7)	1.931(3)
Ga(1)-O(5)	2.017(3)
Ga(1)-O(4)	2.116(3)
Ga(2)-O(9)	1.900(3)
Ga(2)-O(1)	1.919(3)
Ga(2)-O(2)	1.923(3)
Ga(2)-O(3)	1.926(2)
Ga(2)-O(4)	2.118(3)
Ga(2)-O(4)#1	2.130(3)
P(3)-O(8)#2	1.521(3)
P(3)-O(9)#3	1.529(3)
P(3)-O(10)	1.534(3)
P(3)-O(2)	1.550(3)
P(4)-O(7)#4	1.511(3)
P(4)-O(6)#1	1.540(3)
P(4)-O(3)#1	1.544(3)
P(4)-O(1)	1.554(2)
O(3)-P(4)#1	1.544(3)
O(4)-Ga(2)#1	2.130(3)
O(6)-P(4)#1	1.540(3)
O(7)-P(4)#5	1.511(3)
O(8)-P(3)#6	1.521(3)
O(9)-P(3)#7	1.529(3)
O(8)-Ga(1)-O(10)	171.86(12)
O(8)-Ga(1)-O(6)	93.74(11)
O(10)-Ga(1)-O(6)	94.35(12)
O(8)-Ga(1)-O(7)	92.62(11)
O(10)-Ga(1)-O(7)	86.74(11)
O(6)-Ga(1)-O(7)	87.43(12)
O(8)-Ga(1)-O(5)	84.01(12)
O(10)-Ga(1)-O(5)	87.86(12)
O(6)-Ga(1)-O(5)	176.09(12)
O(7)-Ga(1)-O(5)	89.48(12)
O(8)-Ga(1)-O(4)	92.45(10)
O(10)-Ga(1)-O(4)	88.62(11)

O(6)-Ga(1)-O(4)	89.60(11)
O(7)-Ga(1)-O(4)	174.28(11)
O(5)-Ga(1)-O(4)	93.68(11)
O(9)-Ga(2)-O(1)	99.05(12)
O(9)-Ga(2)-O(2)	86.52(11)
O(1)-Ga(2)-O(2)	95.18(11)
O(9)-Ga(2)-O(3)	91.49(12)
O(1)-Ga(2)-O(3)	164.57(11)
O(2)-Ga(2)-O(3)	96.69(11)
O(9)-Ga(2)-O(4)	176.46(11)
O(1)-Ga(2)-O(4)	84.33(11)
O(2)-Ga(2)-O(4)	94.25(11)
O(3)-Ga(2)-O(4)	84.99(11)
O(9)-Ga(2)-O(4)#1	91.25(11)
O(1)-Ga(2)-O(4)#1	84.58(10)
O(2)-Ga(2)-O(4)#1	177.70(11)
O(3)-Ga(2)-O(4)#1	83.95(10)
O(4)-Ga(2)-O(4)#1	88.01(11)
O(8)#2-P(3)-O(9)#3	112.65(15)
O(8)#2-P(3)-O(10)	107.23(15)
O(9)#3-P(3)-O(10)	111.61(16)
O(8)#2-P(3)-O(2)	107.90(16)
O(9)#3-P(3)-O(2)	107.32(15)
O(10)-P(3)-O(2)	110.08(15)
O(7)#4-P(4)-O(6)#1	109.46(15)
O(7)#4-P(4)-O(3)#1	112.00(16)
O(6)#1-P(4)-O(3)#1	109.22(15)
O(7)#4-P(4)-O(1)	106.90(15)
O(6)#1-P(4)-O(1)	109.08(16)
O(3)#1-P(4)-O(1)	110.11(14)
P(4)-O(1)-Ga(2)	127.04(15)
P(3)-O(2)-Ga(2)	131.28(17)
P(4)#1-O(3)-Ga(2)	126.73(16)
Ga(1)-O(4)-Ga(2)	124.09(12)
Ga(1)-O(4)-Ga(2)#1	122.58(12)
Ga(2)-O(4)-Ga(2)#1	91.99(11)
P(4)#1-O(6)-Ga(1)	122.92(15)
P(4)#5-O(7)-Ga(1)	153.18(17)
P(3)#6-O(8)-Ga(1)	144.06(18)
P(3)#7-O(9)-Ga(2)	132.51(16)
P(3)-O(10)-Ga(1)	138.41(17)

Table 4. Bond lengths [Å] and angles [^{0}] for stan198.
Symmetry transformations used to generate equivalent atoms:
#1 -x,-y+1,-z+2 #2 x-1/2,-y+1/2,z-1/2
#3 -x-1/2,y-1/2,-z+3/2 #4 x-1/2,-y+1/2,z+1/2
#5 x+1/2,-y+1/2,z-1/2 #6 x+1/2,-y+1/2,z+1/2
#7 -x-1/2,y+1/2,-z+3/2

	U11	U22	U33	U23	U13	U12
Ga(1)	3(1)	2(1)	4(1)	0(1)	0(1)	0(1)
Ga(2)	2(1)	2(1)	4(1)	0(1)	0(1)	0(1)
P(3)	3(1)	2(1)	4(1)	0(1)	0(1)	0(1)

P(4)	2(1)	2(1)	5(1)	0(1)	1(1)	0(1)
O(1)	5(1)	5(1)	5(1)	0(1)	1(1)	-3(1)
O(2)	6(1)	3(2)	6(1)	-2(1)	1(1)	1(1)
O(3)	3(1)	5(1)	7(1)	1(1)	1(1)	1(1)
O(4)	4(1)	7(2)	6(1)	0(1)	2(1)	-1(1)
O(5)	6(1)	8(2)	16(1)	3(1)	2(1)	0(1)
O(6)	5(1)	3(1)	6(1)	-1(1)	2(1)	0(1)
O(7)	6(1)	10(2)	6(1)	-1(1)	2(1)	3(1)
O(8)	7(1)	4(1)	5(1)	1(1)	-1(1)	2(1)
O(9)	9(1)	3(1)	6(1)	1(1)	2(1)	2(1)
O(10)	5(1)	6(2)	8(1)	0(1)	2(1)	2(1)
OW1	14(1)	7(2)	12(1)	-1(1)	5(1)	0(1)
OW2	14(1)	17(2)	13(1)	2(1)	4(1)	1(1)

Table 5. Anisotropic displacement parameters ($Å^2$ x 10^3) for stan198.
The anisotropic displacement factor exponent takes the form:
$-2\ pi^2\ [\ h^2\ a^{*2}\ U11 + ... + 2\ h\ k\ a^*\ b^*\ U12\ ]$

	x	y	z	U(eq)
Ga(1)	1017(1)	2326(1)	8156(1)	3(1)
Ga(2)	-1134(1)	5425(1)	8708(1)	3(1)
P(3)	-2070(1)	3155(1)	6324(1)	3(1)
P(4)	-2028(1)	4658(1)	11490(1)	3(1)
O(1)	-2386(3)	4814(3)	9861(2)	5(1)
O(2)	-2204(3)	4592(3)	7004(3)	6(1)
O(3)	506(3)	5911(3)	7995(3)	5(1)
O(4)	3(3)	3582(3)	9420(2)	5(1)
O(5)	-37(3)	590(3)	8482(3)	10(1)
O(6)	2136(3)	3908(3)	7839(3)	5(1)
O(7)	1873(3)	1309(3)	6852(3)	7(1)
O(8)	2399(3)	1694(3)	9740(3)	6(1)
O(9)	-2052(3)	7120(3)	8035(3)	6(1)
O(10)	-505(3)	2720(3)	6595(3)	6(1)
OW1	1793(3)	-1467(3)	9629(3)	11(1)
OW2	-114(3)	8087(4)	6020(3)	14(1)

Table 6. Atomic coordinates (x10^4) and equivalent isotropic displacement parameters ($Å^2$ x 10^3) for stan198.
U(eq) is defined as one third of the trace of the orthogonalized Uij tensor

7.3 Crystal Data: lprm3n

Hg(1)-Cl(2)	2.402(5)
Hg(1)-Cl(1)	2.414(4)
Hg(1)-Cl(3)	2.429(5)
Hg(1)-Cl(6)	2.896(5)
Hg(2)-Cl(4)	2.403(5)

Hg(2)-Cl(5)	2.421(6)
Hg(2)-Cl(6)#1	2.431(5)
Hg(2)-Cl(3)	2.907(5)
Cl(6)-Hg(2)#2	2.431(5)
N(1)-C(3)	1.46(2)
N(1)-C(4)	1.51(3)
N(1)-C(2)	1.49(2)
N(1)-C(1)	1.50(3)
N(2)-C(7)	1.45(4)
N(2)-C(8)	1.47(3)
N(2)-C(6)	1.49(3)
N(2)-C(5)	1.49(3)
Cl(2)-Hg(1)-Cl(1)	119.9(2)
Cl(2)-Hg(1)-Cl(3)	119.2(2)
Cl(1)-Hg(1)-Cl(3)	120.4(2)
Cl(2)-Hg(1)-Cl(6)	95.7(2)
Cl(1)-Hg(1)-Cl(6)	92.03(17)
Cl(3)-Hg(1)-Cl(6)	89.92(17)
Cl(4)-Hg(2)-Cl(5)	120.8(2)
Cl(4)-Hg(2)-Cl(6)#1	123.2(2)
Cl(5)-Hg(2)-Cl(6)#1	115.6(2)
Cl(4)-Hg(2)-Cl(3)	91.12(17)
Cl(5)-Hg(2)-Cl(3)	93.0(2)
Cl(6)#1-Hg(2)-Cl(3)	92.27(17)
Hg(1)-Cl(3)-Hg(2)	96.61(18)
Hg(2)#2-Cl(6)-Hg(1)	95.25(18)
C(3)-N(1)-C(4)	110.5(19)
C(3)-N(1)-C(2)	109.6(17)
C(4)-N(1)-C(2)	107.9(16)
C(3)-N(1)-C(1)	107.2(18)
C(4)-N(1)-C(1)	108(2)
C(2)-N(1)-C(1)	113.3(18)
C(7)-N(2)-C(8)	109(2)
C(7)-N(2)-C(6)	115(2)
C(8)-N(2)-C(6)	109.2(16)
C(7)-N(2)-C(5)	105(2)
C(8)-N(2)-C(5)	108(2)
C(6)-N(2)-C(5)	111(2)

Table 7. Bond lengths [Å] and angles [^{0}] for lprm3.
Symmetry transformations used to generate equivalent atoms:
#1 x-1,y,z #2 x+1,y,z

	x	y	z	U(eq)
Hg(1)	4586(1)	2511(1)	8300(1)	57(1)
Hg(2)	-533(1)	2961(1)	7149(1)	59(1)
Cl(1)	5693(7)	2112(4)	5903(5)	58(1)
Cl(2)	5014(7)	1574(4)	10435(6)	63(1)
Cl(3)	2680(7)	3749(4)	8484(7)	67(2)
Cl(4)	799(7)	1571(4)	7363(6)	60(1)
Cl(5)	-441(8)	3777(5)	4837(6)	73(2)
Cl(6)	7666(7)	3564(4)	9062(7)	73(2)
N(1)	4480(20)	4470(11)	3076(17)	50(4)
N(2)	9830(20)	6249(11)	7549(15)	46(4)

C(1)	4550(40)	3528(16)	2770(30)	85(8)
C(2)	2810(30)	4883(16)	2440(30)	68(7)
C(3)	4630(30)	4580(17)	4720(20)	64(6)
C(4)	6030(30)	4888(18)	2360(30)	89(9)
C(5)	9800(40)	5640(20)	8840(30)	100(10)
C(6)	11320(30)	6050(20)	6580(30)	96(10)
C(7)	9900(40)	7090(20)	8230(40)	103(10)
C(8)	8130(30)	6160(30)	6650(30)	137(16)

Table 8. Atomic coordinates (x 10^4) and equivalent isotropic displacement parameters (Å^2 x 10^3) for lprm3.
U(eq) is defined as one third of the trace of the orthogonalized Uij tensor.

	U11	U22	U33	U23	U13	U12
Hg(1)	65(1)	54(1)	53(1)	4(1)	13(1)	8(1)
Hg(2)	66(1)	57(1)	55(1)	5(1)	9(1)	11(1)
Cl(1)	63(3)	64(3)	49(3)	-1(2)	21(2)	4(3)
Cl(2)	62(3)	68(4)	59(3)	15(3)	0(2)	-3(3)
Cl(3)	47(3)	59(3)	92(4)	-25(3)	-11(3)	15(3)
Cl(4)	62(3)	54(3)	62(3)	-3(2)	-3(2)	16(3)
Cl(5)	66(4)	98(5)	55(3)	22(3)	1(3)	-12(3)
Cl(6)	55(3)	72(4)	96(4)	-29(3)	30(3)	-15(3)
N(1)	68(12)	39(10)	42(9)	5(7)	1(8)	0(8)
N(2)	52(10)	55(11)	30(7)	-4(7)	15(7)	12(8)
C(1)	150(30)	37(14)	67(14)	-19(12)	-11(14)	-9(15)
C(2)	38(12)	80(17)	82(15)	37(13)	-13(11)	11(11)
C(3)	59(14)	87(18)	44(11)	1(11)	-9(10)	-13(13)
C(4)	54(14)	90(20)	130(20)	61(18)	39(14)	1(13)
C(5)	130(30)	90(20)	88(18)	40(16)	64(17)	26(18)
C(6)	45(14)	180(30)	64(15)	-17(18)	15(11)	-13(17)
C(7)	90(19)	68(19)	160(30)	-5(18)	40(20)	12(16)
C(8)	42(14)	290(50)	74(17)	-70(20)	-9(13)	0(20)

Table 9. Anisotropic displacement parameters (Å^2 x 10^3) for lprm3.
The anisotropic displacement factor exponent takes the form:
$-2\pi^2 [h^2 a^{*2} U11 + ... + 2 h k a^* b^* U12]$

7.4 Crystal Data: lprm3p

Hg(1)-Cl(1)	2.459(12)
Hg(1)-Hg(1)#1	2.532(3)
Cl(1)-Hg(1)-Hg(1)#1	178.8(5)

Table 10. Bond lengths [Å] and angles [^{0}] for lprm34.
Symmetry transformations used to generate equivalent atoms:
#1 -x+1,y,-z+1

	U11	U22	U33	U23	U13	U12
Hg(1)	23(2)	33(2)	36(2)	-1(2)	10(1)	3(2)
Cl(1)	22(3)	22(3)	22(3)	0(1)	8(1)	0(1)

Table 11. Anisotropic displacement parameters (A^2 x 10^3) for lprm34.
The anisotropic displacement factor exponent takes the form:
$-2\ pi^2\ [\ h^2\ a^{*2}\ U11 + ... + 2\ h\ k\ a^*\ b^*\ U12$

	x	y	z	U(eq)
Hg(1)	3838(2)	6930(40)	3831(4)	31(2)
Cl(1)	1580(12)	7030(40)	1500(30)	22(3)

Table 12. Atomic coordinates (x 10^4) and equivalent isotropic displacement parameters (Å^2 x 10^3) for lprm34.
U(eq) is defined as one third of the trace of the orthogonalized Uij tensor.

7.5 Crystal Data: lprm4

N(1)-C(6)	1.316(6)
N(1)-C(2)	1.319(7)
C(2)-C(3)	1.376(8)
C(3)-C(4)	1.361(7)
C(4)-C(5)	1.377(6)
C(4)-C(4')	1.523(7)
C(5)-C(6)	1.386(8)
N(1')-C(2')	1.326(6)

N(1')-C(6')	1.344(6)
C(2')-C(3')	1.381(7)
C(3')-C(4')	1.391(6)
C(4')-C(5')	1.386(6)
C(5')-C(6')	1.368(7)
C(6)-N(1)-C(2)	118.1(4)
N(1)-C(2)-C(3)	122.8(5)
C(4)-C(3)-C(2)	119.9(5)
C(3)-C(4)-C(5)	117.3(5)
C(3)-C(4)-C(4')	121.2(4)
C(5)-C(4)-C(4')	121.6(4)
C(4)-C(5)-C(6)	119.6(5)
N(1)-C(6)-C(5)	122.4(4)
C(2')-N(1')-C(6')	118.4(4)
N(1')-C(2')-C(3')	122.6(4)
C(2')-C(3')-C(4')	119.6(4)
C(5')-C(4')-C(3')	116.9(4)
C(5')-C(4')-C(4)	121.6(4)
C(3')-C(4')-C(4)	121.5(4)
C(6')-C(5')-C(4')	120.4(5)
N(1')-C(6')-C(5')	122.1(5)

Table 13. Bond lengths [Å] and angles [^{0}] for lprm4

	x	y	z	U(eq)
Cl(1)	3726(1)	2500	7375(1)	107(1)
N(1)	5083(4)	2500	4693(2)	32(1)
C(2)	5793(6)	2500	3979(4)	68(2)
C(3)	7200(6)	2500	3962(3)	60(2)
C(4)	7917(5)	2500	4704(3)	24(1)
C(5)	7177(5)	2500	5450(3)	45(2)
C(6)	5760(5)	2500	5416(3)	44(2)
N(1')	12322(4)	2500	4712(3)	32(1)
C(2')	11627(5)	2500	5436(3)	34(1)
C(3')	10215(5)	2500	5463(3)	29(1)
C(4')	9475(5)	2500	4707(3)	25(1)
C(5')	10220(5)	2500	3957(3)	42(2)
C(6')	11619(5)	2500	3977(4)	50(2)
O(1)	6255(3)	-157(7)	7303(3)	107(2)

Table 14. Atomic coordinates (x10^4) and equivalent isotropic displacement parameters (Å^2 x10^3) for lprm4.
U(eq) is defined as one third of the trace of the Orthogonalized Uij tensor

	U11	U22	U33	U23	U13	U12
Cl(1)	18(1)	274(3)	28(1)	0	2(1)	0
N(1)	24(2)	43(3)	28(3)	0	0(2)	0
C(2)	34(4)	149(7)	21(3)	0	-1(3)	0
C(3)	27(3)	134(7)	19(3)	0	5(2)	0
C(4)	27(3)	27(2)	19(2)	0	0(2)	0
C(5)	23(3)	89(5)	24(3)	0	0(2)	0
C(6)	29(3)	81(5)	24(3)	0	5(2)	0
N(1')	21(2)	49(3)	26(3)	0	0(2)	0
C(2')	36(3)	39(3)	26(3)	0	-5(2)	0
C(3')	25(3)	39(3)	21(3)	0	-1(2)	0
C(4')	28(3)	27(3)	22(3)	0	-3(2)	0
C(5')	25(3)	80(5)	21(3)	0	-3(2)	0
C(6')	34(4)	90(5)	24(3)	0	4(2)	0
O(1)	91(3)	158(4)	70(3)	36(3)	0(2)	-4(2)

Table 15. Anisotropic displacement parameters ($Å^2$ x 10^3) for lprm4.
The anisotropic displacement factor exponent takes the form:
$-2\ pi^2\ [\ h^2\ a^{*2}\ U11 + ... + 2\ h\ k\ a^*\ b^*\ U12\ ]$

7.6 Crystal Data: lprm6

Ga(1)-O(1)#1	1.805(4)
Ga(1)-O(1)	1.805(4)
Ga(1)-O(2)	1.818(4)
Ga(1)-O(2)#1	1.818(4)
O(1)-P(1)	1.526(4)
O(2)-P(1)#2	1.524(5)
P(1)-O(2)#3	1.524(5)
P(1)-O(2)#4	1.524(5)
P(1)-O(1)#5	1.526(4)
O(1)#1-Ga(1)-O(1)	112.2(3)
O(1)#1-Ga(1)-O(2)	110.20(19)
O(1)-Ga(1)-O(2)	105.22(16)
O(1)#1-Ga(1)-O(2)#1	105.22(16)
O(1)-Ga(1)-O(2)#1	110.20(19)
O(2)-Ga(1)-O(2)#1	114.0(3)
P(1)-O(1)-Ga(1)	135.5(3)
P(1)#2-O(2)-Ga(1)	134.7(3)
O(2)#3-P(1)-O(2)#4	108.1(4)
O(2)#3-P(1)-O(1)#5	108.2(2)
O(2)#4-P(1)-O(1)#5	111.4(2)
O(2)#3-P(1)-O(1)	111.4(2)
O(2)#4-P(1)-O(1)	108.2(2)
O(1)#5-P(1)-O(1)	109.5(4)

Table 16. Bond lengths [Å] and angles [^{0}] for lprm6.
Symmetry transformations used to generate equivalent atoms:

#1 y,x,-z #2 x+1,y,z #3 -x+1,-x+y+1,-z+1/3
#4 x-1,y,z #5 -x,-x+y,-z+1/

	U11	U22	U33	U23	U13	U12
Ga(1)	9(1)	9(1)	7(1)	0(1)	0(1)	5(1)
O(1)	12(2)	20(2)	10(2)	-1(2)	1(2)	8(2)
O(2)	10(2)	19(2)	12(2)	-3(2)	-2(2)	11(2)
P(1)	7(1)	8(1)	6(1)	0(1)	0(1)	4(1)

Table 17. Anisotropic displacement parameters ($Å^2$ x 10^3) for lprm6. The anisotropic displacement factor exponent takes the form: $-2\pi^2 [h^2 a^{*2} U11 + ... + 2 h k a^* b^* U12]$

	x	y	z	U(eq)
Ga(1)	4565(2)	4565(2)	0	8(1)
O(1)	923(11)	4096(11)	595(4)	14(1)
O(2)	7277(10)	5896(11)	1274(4)	12(1)
P(1)	0	5432(5)	1667	7(1)

Table 18. Atomic coordinates (x 10^4) and equivalent isotropic displacement parameters (A^2 x 10^3) for lprm6. U(eq) is defined as one third of the trace of the orthogonalized Uij tensor.

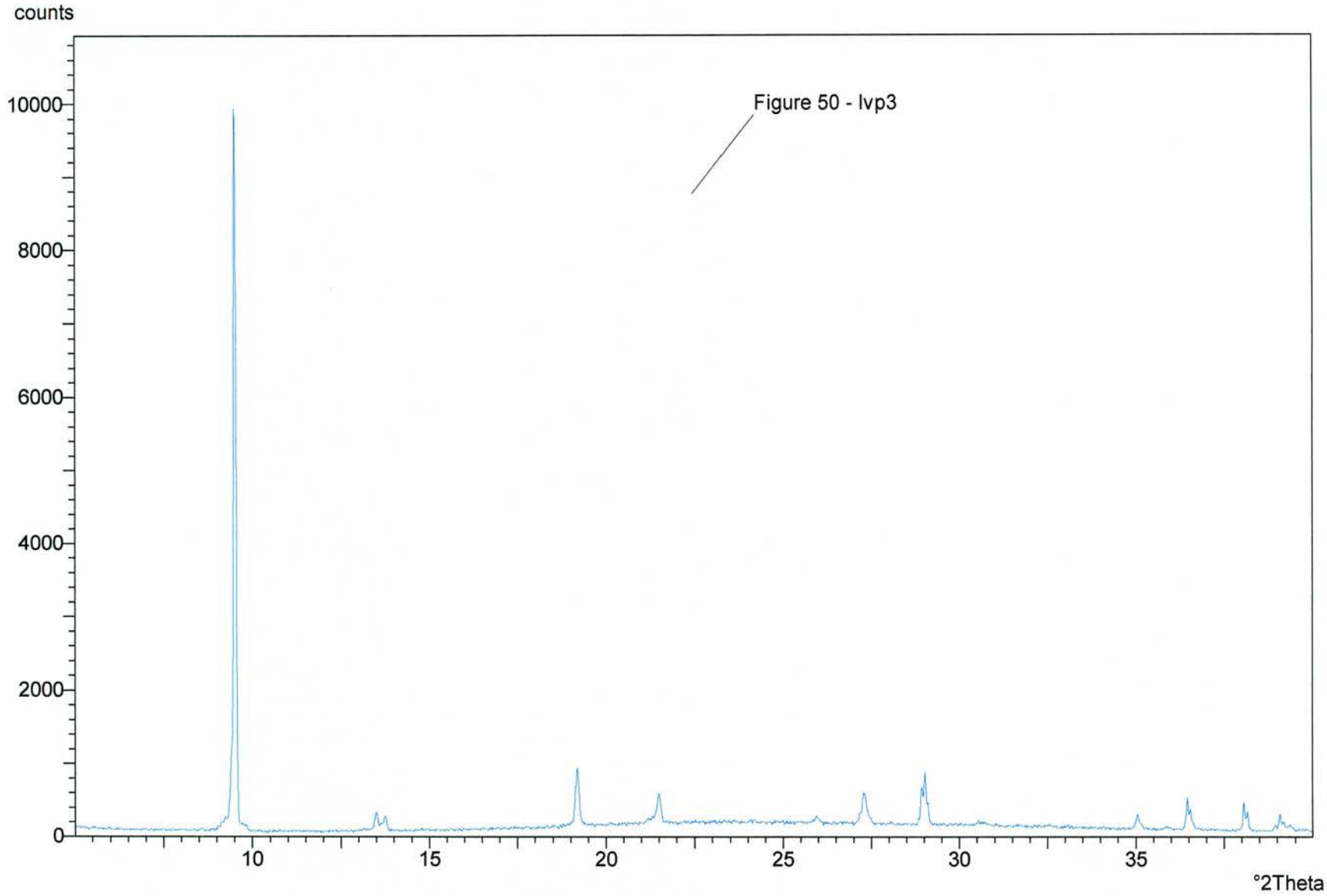

Figure 50 - lvp3

Figure 51 - lvp16 overnight

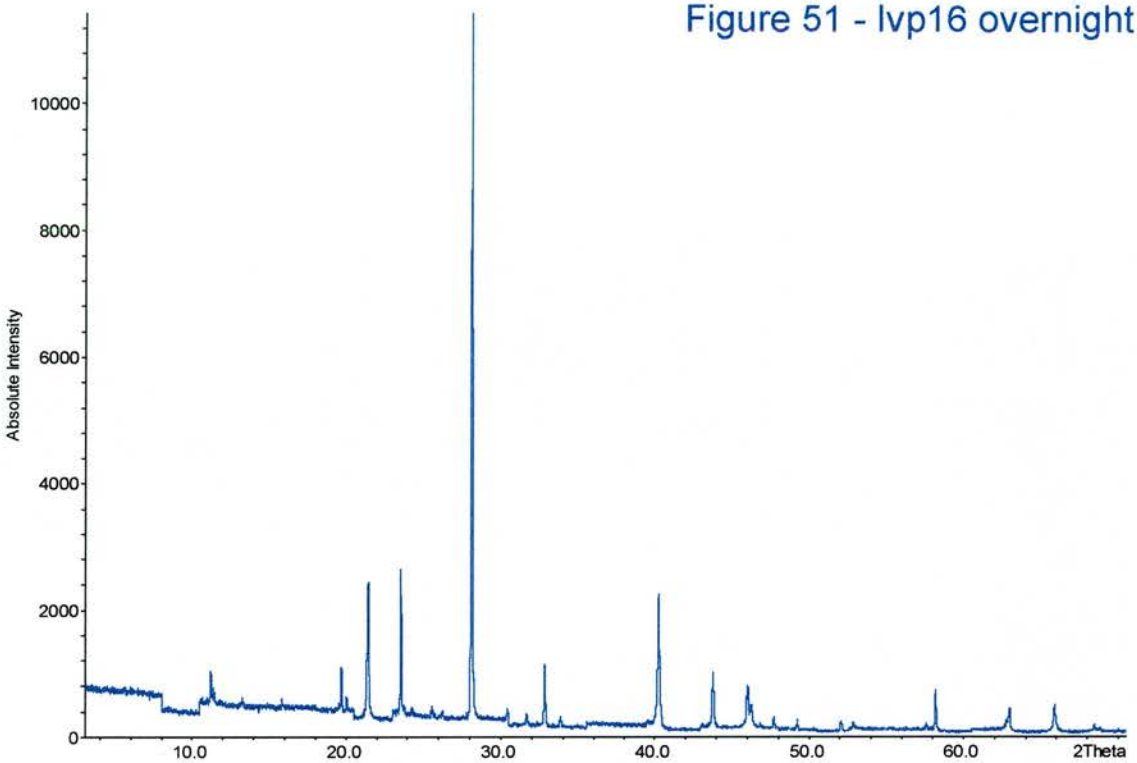

Figure 52 – $HgCl_2$

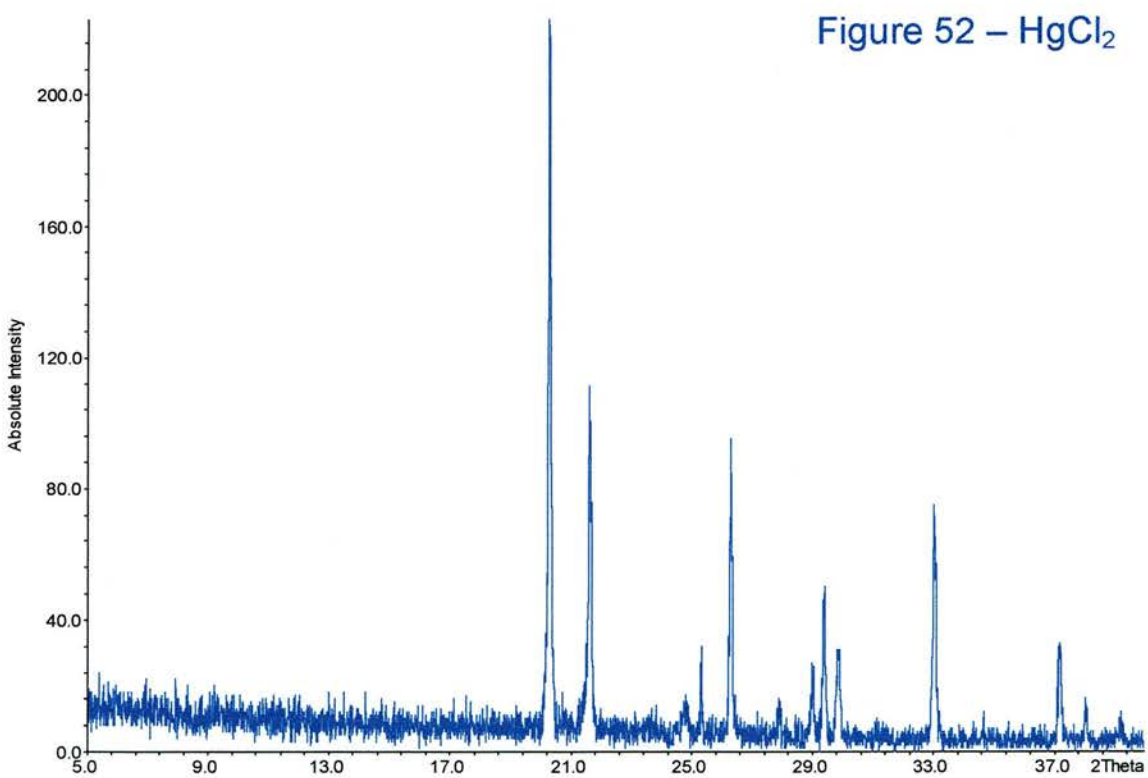

Figure 53 - lvp51